Energy 313 (2024) 133653

Contents lists available at ScienceDirect

Energy

journal homepage: www.elsevier.com/locate/energy

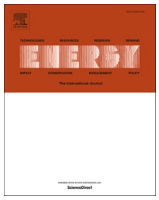

Techno-economic analysis of hybrid renewable energy systems for cost reduction and reliability improvement using dwarf mongoose optimization algorithm

Saleh Al Dawsari [a,b,*], Fatih Anayi [a], Michael Packianather [a]

[a] School of Engineering, Cardiff University, Cardiff, CF24 3AA, UK
[b] Electrical Engineering Department, College of Engineering, Najran University, Najran, Saudi Arabia

ARTICLE INFO

Keywords:
Hybrid power plants
Reliability assessment
DMOA
Net present cost (NPC)
LCOE

ABSTRACT

The global energy crisis, particularly in isolated and remote regions, has increased interest in renewable energy sources (RESs) to meet growing energy demands. Integrating RESs with energy storage systems offers a promising solution to mitigate fluctuations and intermittency, but concerns about cost and reliability remain. This study explores the optimal design of various microgrid configurations, combining photovoltaic (PV), wind turbine (WT), battery energy storage system (BESS), and diesel generator (DG) systems for Najran city, Saudi Arabia, via real-world meteorological and load demand data. The Dwarf Mongoose Optimization Algorithm (DMOA), alongside the salp swarm algorithm (SSA) and whale optimization algorithm (WOA), was applied to minimize the levelized cost of energy (LCOE) while improving system reliability. The results demonstrate that the PV/BESS configuration, although cost-effective with an LCOE of 0.038 USD/kWh, fail to meet reliability constraints with a loss of power supply probability (LPSP) of 0.679. In contrast, the PV, WT, BESS, and DG configurations achieved an LPSP of 1.9 × 10^–8% with an LCOE of 0.199 USD/kWh, offering a robust and reliable solution for the region's energy needs. This paper presents a novel application of the DMOA for optimizing hybrid renewable energy systems, demonstrating its effectiveness in achieving a balance between cost and reliability. This strategy provides a viable approach for sustainable energy planning in similar regions facing energy challenges.

Abbreviations and Symbols

MSOT	Modified Seagull Optimization Technique	BG	Biomass Gasifier
SOA	Seagull Optimization Algorithm	NPC	Net Present Cost
MFFA	Modified Farmland Fertility Algorithm	LCOE	Levelized Cost Of Energy
DMGWO	Discrete Multiobjective Wolf Algorithm	LPSP	Loss Of Power Supply Probability
cEHO	constraint Elephant Herd Optimization Algorithm	LPS	loss of power supply
JAYA	Jaya algorithm	P_{dummy}	dummy load
PSO	Particle Swarm Optimization.	SEC	Saudi Electricity Company
BSA	Backtracking Search Algorithm	$p_{PV}(t)$	Power produced by each individual PV panel
GA	Genetic Algorithm	P_{PV}	PV generated power
MOA	Mayfly Optimization Algorithm	R	Solar radiation
IAOA	improved Arithmetic Optimization Algorithm	R_{ref}	Solar radiation under reference conditions
AO	Aquila Optimizer	$P_{R,PV}$	Rated power of the PV panel
AOA	Original Arithmetic Optimization Algorithm	N_T	Photovoltaic panel's temperature coefficient
DMOA	Dwarf Mongoose Optimization Algorithm	T_{ref}	Temperature under reference conditions
SSA	Salp Swarm Algorithm	T_c	Cell temperature
IHOGA	Improved Hybrid Optimization by Genetic Algorithms	T_{air}	Air temperature in the metrological data of the site
WOA	whale Optimization Algorithm	R_a	Radiation

(continued on next column)

(continued)

(continued on next page)

* Corresponding author. School of Engineering, Cardiff University, Cardiff, CF24 3AA, UK.
E-mail addresses: aldawsarisa@cardiff.ac.uk (S. Al Dawsari), anayi@cardiff.ac.uk (F. Anayi), packianatherms@cardiff.ac.uk (M. Packianather).

https://doi.org/10.1016/j.energy.2024.133653
Received 10 July 2024; Received in revised form 12 October 2024; Accepted 27 October 2024
Available online 2 November 2024

(*continued*)

NSGA-II	Nondominated Sorting Genetic Algorithm	NOCT	Operating cell temperature
TLBO	Teaching-Learning-Based Optimization	N_{PV}	Number of PV
CSA	Chameleon Swarm Algorithm	P_{WT}	Generated power output of individual wind turbines
GWO	Gray Wolf Optimization	$P_{R,WT}$	Nominal power of a wind turbine
SOA	Seagull Optimization Algorithm	V	Wind speed
STOA	Sooty Tern Optimization Algorithm	V_{IN}	Cut in speed
SCA	Sine Cosine Algorithm	V_{UP}	Cut out speed
HS	Harmony Search	V_R	Wind speed associated with the nominal power
EMS	Energy Management Strategy	C_P	Power coefficient of the WT
RESs	Renewable Energy Sources	ρ_a	Air density
HRES	Hybrid Renewable Energy System	A_{WT}	Swept area
GHG	Greenhouse Gas	η_{WT}	Efficiency of the WT
PV	Photovoltaic	SOC	State of charge
WT	Wind Turbine	$SOC_{\min}$	Minimum state of the charge threshold
BESS	Battery Energy Storage System	$SOC_{\max}$	Maximum state of the charge threshold
DG	Diesel Generator	E_{CH}	Charging energy
FC	Fuel Cell	E_{DIS}	Discharging energy
C_{f_DG}	Fuel consumption (L/h).	P_L	Load demand
$P_{DG}(t)$	DG power (kW)	σ	Rate of self-discharge
P_{rated_DG}	Rated power of the DG (kW)	η_{dis}	Discharging efficiency
α_{DG} and β_{DG}	Consumption coefficient curve of the DG	η_{ch}	Charging efficiency
C_{DG}	Yearly fuel cost	$C_{Mnt-BAT}$	Yearly maintenance cost per battery
CF	Unit fuel cost	C_{BAT}	Unit cost per battery
LCC	Life cycle cost	$C_{Conv/Inv}$	Present value of the converter/inverter components,
AM	Yearly maintenance cost	$P_{Conv/Inv}$	Price of the converter/inverter
AC	capital cost	C_{Mnt-DG}	Yearly maintenance cost of each diesel generator
AM_{PV}	PV annual maintenance costs	C_{DG}	Unit cost of each diesel generator
AC_{PV}	PV capital costs	DOD	Maximum depth of discharge
C_{Mnt-PV}	PV yearly maintenance cost	S_{BAT}	Nominal capacity of the storage system
C_{PV}	Unit cost of each PV panel	R_f	Renewable energy fraction
C_{WT}	Unit cost of each wind turbine	E_{ren}	Total renewable energy
C_{Mnt-WT}	Yearly maintenance cost of each wind turbine	E_{tot}	Total Annual Energy Consumption
n	Life of the system	Q_{CO}	Total CO_2 emission amount (Kgco2 /*year*)
i_r	Interest rate	$TotalC_{f\_DG}$	Total yearly fuel consumption (*litre*/*year*)
X	Possible population of mongooses	EF	Emission factor for the fuel (Kgco2/Litre)
$x_{i,j}$	Spatial location of the *jth* dimension within the *ith* population.	NPC	Net present cost
n	size of the population	$AREP$	Replacement Cost
d	dimension of the problem	UB	Upper Bound
Var_{Min} and Var_{Max}	Lower and upper bounds of each problem variable, respectively.	LB	Lower Bound
Var_{Size}	Size of the choice variables or the dimensions of the problem	bs	number of babysitters

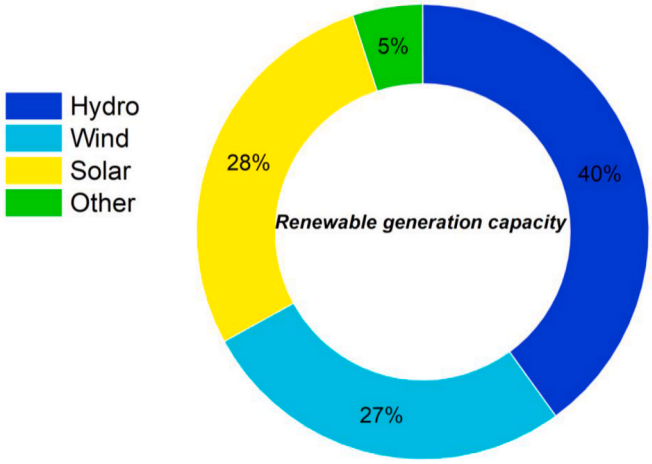

Fig. 1. Renewable generation capacity by energy source as of 2021.

1. Introduction

Numerous countries have robust policies for promoting renewable energy [1], as fossil fuel supplement disruptions highlight the advantages of domestically produced renewable electricity in terms of energy security. Moreover, the high prices of fossil fuels worldwide make solar and wind viable alternatives to other fuel sources [2,3]. By the end of 2021, the worldwide renewable energy capacity had reached 3064 GW [4]. According to Fig. 1, hydropower production has the highest capacity at 1230 GW, whereas the solar and wind energy capacities are 849 GW and 825 GW, respectively. Furthermore, other renewables produce 143 GW from bioenergy, 16 GW from geothermal energy, and 524 MW from marine energy [4,5].

The urgency of expanding renewable energy sources is particularly crucial for reducing greenhouse gas emissions, ensuring energy reliability, and reaching underserved areas [6]. In Saudi Arabia, while crude oil remains the dominant energy source, there is a noticeable shift toward renewable energy, despite the initially higher costs. The Kingdom's abundant solar and wind resources provide significant potential to reduce dependence on fossil fuels, curb CO2 emissions, and stimulate economic growth through job creation and energy diversification [7]. This aligns with global trends where solar and wind energy are becoming viable alternatives as renewable energy capacity worldwide continues to expand.

The Saudi Electricity Company (SEC) has also made significant strides toward a cleaner energy mix, with plans to phase out liquid fuels entirely by 2030 and increase its renewable energy capacity to 19 GW by 2025. These initiatives are part of a broader trend of integrating renewable energy into national grids, which is a critical step toward reducing environmental impacts and enhancing energy security in the face of volatile global energy markets [8].

The demand for electricity in Saudi Arabia has been growing at an annual rate of 8 %, which necessitates substantial investments in new energy capacity. As part of its Vision 2030 goals, Saudi Arabia has committed to substantial renewable energy projects, with plans to install up to 200 GW of solar power by 2030. These projects not only address rising energy demands but also have the potential to create 80,000 jobs, boosting the local economy [7]. Such efforts illustrate Saudi Arabia's alignment with the global energy transition, where renewables are increasingly seen as essential for long-term energy security and sustainability.

The potential of hybrid power plants, which integrate renewable sources such as solar, wind, and BESS, is emerging as a key solution to the challenges of energy reliability and cost efficiency. The cost of renewable technologies continues to decline, making hybrid systems an increasingly attractive option for both developed and developing

countries [9]. These systems ensure the provision of reliable energy, with the added benefit of reducing emissions and relying on conventional fuels.

While microgrids offer numerous advantages, such as reduced maintenance costs, emissions, and increased reliability and flexibility, their initial investment costs tend to be higher than those of conventional power systems. Consequently, recent research has focused on finding cost-effective ways to determine microgrids' optimal size and configuration. In line with previous studies, researchers worldwide have increasingly recognized the importance of optimizing microgrid systems with hybrid power sources. Many scholars have developed optimization techniques to identify optimal microgrid operating points and configurations. These optimization methods typically involve minimizing costs and emissions or maximizing system reliability. In this context, the DMOA is an emerging metaheuristic algorithm that has demonstrated effective performance in solving complex, nonlinear, and optimization problems. Its unconventional approach combines both exploration and exploitation phases, enabling it to balance the global search for optimal solutions while avoiding local minima, which is crucial for systems with nonlinear constraints such as those found in energy and resource management. The primary contributions of the research outlined in this paper are summarized as follows.

- This paper presents a comprehensive modeling approach to determine the optimal configuration of a standalone microgrid system designed to meet the demand load of a residential area in Najran city, KSA. This system incorporates solar panels, wind turbines, BESSs, and diesel generators, and the effectiveness of the approach is carefully considered.
- An energy management strategy (EMS) that manages the power flow between different RESs is presented.
- The analysis is performed on real solar radiation, wind speed and temperature data recorded for the Najran region in southern Saudi Arabia. This study takes a significant step toward addressing a real power shortage problem in a region in Najran city, KSA, by applying the DOMA algorithm to optimize system components. The use of real-time meteorological data from the site further enhances the practical relevance of the research, making the audience feel the immediate impact of the study.
- To the authors' knowledge, applying the DOMA optimization algorithm for designing RES microgrids has not been previously reported in the literature. Moreover, this paper conducts a comprehensive comparison of the DOMA results with those obtained from other algorithms, accompanied by a thorough discussion and analysis. Additionally, various configurations obtained through the optimization process have been meticulously analyzed and compared.
- The optimization criterion aims to achieve the minimum total cost of the system, ensuring reliability and thereby offering tangible benefits for real-world applications.

The subsequent section of the present study is organized in a sequential manner. Section 2 reviews previous studies related to the optimization of energy systems. Section 3 provides a comprehensive overview of the research methodology employed, with a specific focus on modeling various energy technologies and methods. Section 4 provides simulation results and discussion. Finally, the study's conclusions are presented and discussed in Section 5.

2. Literature review

The increasing adoption of renewable energy also necessitates the optimization of energy systems to ensure cost effectiveness and reliability. The optimal configurations for RES systems rely on mature commercial technologies and robust metaheuristic intelligent optimization techniques [10,11]. For example, the HOMER platform was extensively utilized in initial research, yielding insights into constructing energy systems that effectively integrate both traditional and renewable energy sources. These hybrid systems, which are enhanced by advanced storage and management techniques, ensure a reliable and cost-efficient supply of energy. One notable example is a microgrid system proposed for rural Iraq, which combines solar panels, hydroelectric power, diesel generators, and batteries. Using HOMER, researchers determined that the optimal configuration would require an estimated expenditure of USD 113,201, demonstrating how optimization techniques can significantly increase the feasibility of such systems [12].

Similarly, an efficient design for a hybrid microgrid system was devised and tested on Kangaroo Island in South Australia. This system integrated solar panels, wind turbines, diesel generators, and batteries, and computer simulations demonstrated that the most effective approach for managing energy consumption was through "load following", a method that adapts energy usage on the basis of fluctuating demands. This approach proved to be the most cost-effective, leading to the lowest overall energy costs over time. HOMER software is pivotal in fine-tuning and optimizing this smart energy configuration [13].

Further research presented a sophisticated approach for designing a small electricity network in El-Qsier, Egypt, using HOMER Pro. The optimal configuration, derived from entirely renewable sources such as solar panels, wind turbines, converters, and batteries, demonstrated how advanced optimization tools could maximize energy reliability and sustainability, even in remote areas [14]. These case studies underscore the importance of optimization platforms such as HOMER in ensuring that renewable energy systems are not only environmentally sustainable but also economically viable. As more countries adopt renewable energy technologies, the use of advanced optimization methods becomes increasingly crucial for achieving cost-efficient, reliable energy solutions.

Similarly, another study [15] proposed a stand-alone system for supplying energy to a small community in Malaysia. This system integrates wind energy, a diesel generator, and batteries to guarantee a reliable power supply. The study results showed that the use of technology such as improved hybrid optimization by genetic algorithm (IHOGA) renewable energy software remains economically feasible and has a beneficial effect on the environment.

Heuristic algorithms are tools that are commonly utilized to fix the optimum sizes of hybrid renewable energy systems [16–18]. The popularity of these algorithms arises from their user-friendly implementation, avoidance of complex mathematical calculations, and ability to explore a broad spectrum of potential solutions, providing flexibility beyond adhering to a single solution pattern [19,20]. Metaheuristic algorithms are characterized by their ability to traverse complex and nonlinear optimization landscapes. Metaheuristic approaches distinguish themselves from conventional optimization techniques because of their ability to handle nonconvex optimization problems effectively, thereby revealing and converging toward global optima. This feature is often lacking in traditional methodologies. The whale optimization algorithm (WOA) demonstrates this feature [21]. This research introduces a simulation model for a hybrid microgrid system that combines solar panels, wind turbines, diesel generators, and batteries. The objective is to determine the optimal dimensions for these components to reduce energy costs and enhance system reliability. Various optimization algorithms, including the whale optimization algorithm, water cycle algorithm, moth-flame optimizer, and hybrid particle swarm-gravitational search algorithm, have been used to optimize microgrid design. The study includes a comprehensive comparison of these algorithms, highlighting the superiority of the hybrid whale optimization algorithm. This analysis utilized precise meteorological information obtained from Abu-Monqar village in Egypt, which was specifically tailored to address the energy requirements of remote areas.

Furthermore, another study [22] examined the optimal sizing procedure for two suggested hybrid solar PV and wind plants in Oman. This study accounted for the disparity in the wind and solar energy potential

Table 1
Summary of recent academic investigations into hybrid energy systems.

Reference	Year	Hybrid system	Site	Optimization Method	Objective Function	Research limitations
[12]	2019	PV/Hydro/Diesel/ Battery	Sakran, Iraq.	HOMER.	NPV	The study did not conduct the validation and comparative analysis of optimization algorithms.
[13]	2021	PV/Wind/Diesel/ Battery.	Kangaroo Island, Australia.	HOMER.	COE	The chosen algorithm needs testing with each different approach used for task assignment.
[14]	2020	PV/WT/Battery.	El-Qsier, Egypt	HOMER Pro.	TNPC, LCOE, LPSP, CEG, JB.	The hybrid systems have not been elaborated upon extensively in the study.
[15]	2020	WT/Diesel/Battery.	Mersing, Malaysis	iHOGA, DIgSILENT, MATLAB Simulink	COE.	The hybrid system does not include solar power, and local renewable resources are not fully utilized.
[21]	2019	PV/Wind/Diesel/ Battery.	Abu-Monqar village, Egypt.	WOA, WCA, MFO, PSOGSA,	COE, LPSP, Pdummy.	The study could explore how the hybrid systems might affect the environment and consider how they could impact the local community in rural areas.
[22]	2015	PV/Wind/Diesel/ Battery.	Al Halaniyat Masirah Islands, oman.	Graphic Construction, Probabilistic, Iterative and Artificial Intelligence,	COE	The article lacks an in-depth exploration of hybrid PV-Wind systems' potential constraints, challenges, and drawbacks.
[23]	2018	PV/WT/Battery.	–	NSGA II	COE, LPSP.	The possible oversight of practical challenges specific to deploying a wind-photovoltaic microgrid for remote/rural telecommunication towers impacts real-world feasibility.
[24]	2021	PV/WT/Battery.	Biskra, Algeria	PSO	LCC	the study's exclusive focus on cost optimization might not fully address the broader practical considerations, such as system reliability.
[25]	2019	PV/Wind/Diesel/ Battery.	–	TLBO	COE, LPSP.	The proposed typical scenario method is dependent on the accuracy and comprehensiveness of historical data, which could impact the effectiveness of microgrid capacity configuration.
[26]	2020	PV/WT/Battery.	–	DMGWO	LCOE, LPSP, and EEG.	Optimal sizing methods for hybrid renewable energy systems could be applied to various microgrid scenarios, and they are contemplating this potential extension.
[27]	2020	PV/WT/ Electrolyzer/FC	Qingdao, China	SOA, MFFA, MSOT	EGC, LPSP	Using electrolyzer/fuel cell/hydrogen based energy storge system could enhance the study's scope yet may introduce complexities in analysis and integration.
[28]	2022	PV/WT/BG/FC	Abu-Monqar, Egypt.	STOA, WOA, SCA, MOA.	EC, LPSP, PEXC.	It could be the absence of a broader analysis involving multiple scenarios with varying parameters.
[29]	2020	PV/WT/FC PV/FC WT/FC	Hawksbayin Pakistan	JAYA GA, BSA and PSO	TAC	The future potential for exploring multiobjective optimization, trade-offs between LPSPmax and TAC, and integrating hybrid energy storage systems using modern meta-heuristic techniques.
[30]	2021	PV, WTs, BG, and pumped hydro storage.	Saudi Arabia.	WOA, FFA, and PSO.	EC	The study's lack of a specific location in Saudi Arabia affects the practicality and relevance of its proposed hybrid energy system.
[31]	2022	PV/WT/Diesel/ Battery	Yalova, Turkey	HSA	ACS	The analysis focuses on evaluating the optimization method's performance without providing specific details on the economic and reliability benefits of the proposed hybrid system.
[32]	2022	PV/Diesel/Battery	China's Gobi Desert	cEHO, HOMER, PSO	NPC, CO2 emissions	The results indicate that the proposed system produces lower carbon emissions compared to the PSO and HOMER-based systems. However, a substantial amount of energy generated by the PV during the day is lost due to the limited battery capacity.
[33]	2022	PV/WT/Diesel/ Battery	El Kharga Oasis, Egypt	IAOA	NPC	The study of the consequences of microgrid systems under various techno-economic configurations is limited.

in Oman. Two case studies are discussed and compared. The electricity costs are determined to be 0.182 USD/kWh and 0.222 USD/kWh for the 12 MW Masirah Island hybrid solar PV and Wind plants, respectively. These results suggest that the hybrid renewable energy system (HRES) is promising in Oman. Solar and wind energy have substantial potential. However, compared with other optimization techniques, iterative and artificial intelligence optimization techniques are more accurate and quicker. The use of similar scenarios in other areas of Oman with high solar PV and wind potential, such as Jabal Alakhdar and Thamrit, is strongly advised.

Moreover, numerous metaheuristic methods, such as the non-dominated sorting genetic algorithm (NSGA-II) [23], particle swarm optimization (PSO) [24], teaching-learning-based optimization (TLBO) [25], the chameleon swarm algorithm (CSA), gray wolf optimization (GWO) [26], and the seagull optimization algorithm (SOA) [27], have been effectively employed to address optimal sizing complexities inherent to hybrid renewable energy systems. These algorithms have proven to be highly effective in solving complex optimization problems and providing practical solutions for the precise sizing of renewable energy components. These solutions often involve the use of energy storage systems, such as lithium-ion batteries and/or fuel cells.

The implementation of metaheuristics has garnered significant attention in various research endeavors, with a focus on achieving optimal configurations for renewable energy systems. For example, a study used a Mayfly Optimization Algorithm (MOA) to optimize PV, biomass gasifier, and fuel cell systems, achieving the lowest energy cost of $0.2107/kWh, with minimal LPSP and greenhouse gas (GHG) emissions. The MOA outperforms other algorithms, such as the STOA, WOA, and SCA, in both cost and environmental impact [28]. Using the Jaya algorithm, the study in Ref. [29] optimized PV, WT, and fuel cell (FC) sizing in a standalone system to minimize consumer costs, considering reliability with $LPSP_{max}$. The results indicated that the PV-FC setup was more favorable at 0 % and 2 % $LPSP_{max}$. The paper is associated with PV-WT-FC and WT-FC. Moreover, the performance of the Jaya algorithm was evaluated against that of other methods. Researcher of [30] optimized a novel hybrid energy system that integrated wind turbines, solar

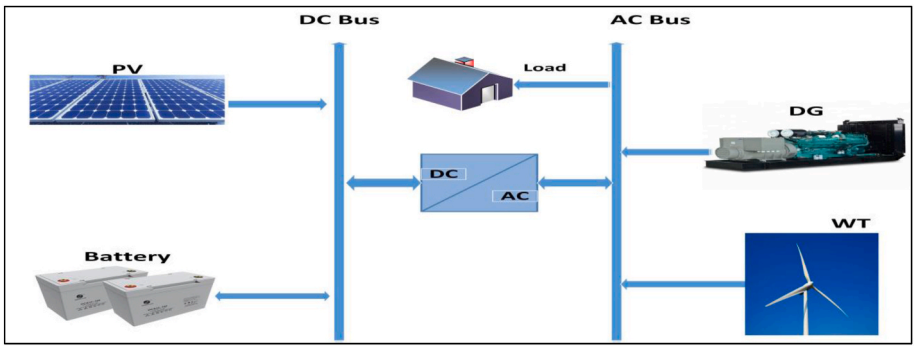

Fig. 2. Conceptual illustration of the proposed renewable energy hybrid PV-Wind-DG-Battery system.

panels, biomass, and pump-hydro storage. By utilizing computational tools, efficient configurations have been developed to minimize costs and environmental impact. A comparison with a battery-integrated system demonstrated the economic viability and efficacy of the proposed hybrid approach.

The study [31] focused mainly on cost-effectiveness and environmental considerations. HRESs beneficial for meeting load requirements, but determining the ideal size is crucial. The Harmony search (HS) algorithm was used to optimize components in the HRES, including solar, wind turbine, battery, diesel generator, and inverter components. A rule-based energy management scheme was proposed to regulate power flow and minimize system costs while meeting energy demand. The simulation results demonstrated that the HS approach exhibited superior performance and convergence characteristics, making it the optimal choice for size.

A study by Ref. [32] proposed a hybrid solar/diesel/battery system in rural areas of China's Gobi Desert. Reducing fuel consumption and pollution were the two primary goals of the system. The constraint approach was used to reduce the complexity of the issue. The optimization procedure employed the elephant herd method (EHO) and its constraint algorithm (cEHO). The simulation results demonstrate that the system meets the load demand, with PV penetration influencing 97.9 % of the total expenses. The cEHO algorithm emits 1735 kg of CO_2 annually, with a startup cost of 48,680 USD.

The paper [33] proposed a new HRES design that includes battery, PV, wind, and diesel generator systems. Considering both technical and ecological factors, the main objective was to reduce the overall net present cost. The improved arithmetic optimization algorithm (IAOA) algorithm was derived by modifying the original arithmetic optimization algorithm (AOA) by incorporating the main operators utilized in the Aquila optimizer (AO). The proposed IAOA enhanced the searchability of a system while mitigating the limitations associated with local search methods. Two hypothetical scenarios for HRES are proposed. The first scenario involved the integration of photovoltaic (PV), wind, diesel, and battery technologies, whereas the second scenario incorporates PV, diesel, and battery technologies. The findings indicated that the suggested IAOA performs better than the other established algorithms do, thus presenting a viable alternative for hybrid renewable energy systems. Table 1 summarizes the system configurations that have been studied on the basis of the academic sources reviewed.

The study presented in this paper investigates diverse energy system scenarios with PV, WT, battery, and DG components. The research uses empirical data, including hourly load demand, irradiation, wind speed, and temperature readings for 2021 in Najran city, Saudi Arabia, to establish a robust framework for addressing substantial-scale energy demands while minimizing costs. The main focus is on optimizing significant-scale energy requirements, aiming to enhance reliability while effectively managing expenditures. Consequently, the DMOA optimization methodology is employed to achieve a dual objective: reducing operational costs while concurrently mitigating the likelihood of power supply disruptions.

Furthermore, a comprehensive comparative analysis that includes different energy system scenarios is rigorously conducted. Each scenario involves specific combinations of PV, DG, and WT sources and BESSs. The primary objective of this analytical investigation is to identify the most economically feasible configuration for a hybrid energy system while carefully considering the critical goal of minimizing the likelihood of power supply shortages. This endeavor is underscored by a thorough examination of each scenario to determine the optimal hybrid energy system configuration that adeptly navigates the intricate balance between cost efficiency and the reliability of the power supply. The incorporation of decision variables, such as the number of wind turbines (N_{wt}), photovoltaic panels (N_{pv}), diesel generators (N_{DG}), and BESS units (N_{bat}), is an essential aspect of this extensive investigation.

3. Methodology and methods

3.1. PV, WT, DG, and battery energy storage system modeling and problem solution size

The PV array, wind turbine, and diesel generator in the standalone PV/WT/DG system are depicted in Fig. 2. They collaborate to generate electricity capable of managing the workload. The batteries are fully charged when the electricity generated by the PV and wind sources equals the power required by the load. The batteries then help provide the primary source of electricity until their stored energy is depleted [21] if the energy generated is insufficient to meet the load's demand. If the power produced by solar panels, wind turbines, and batteries is insufficient to meet the required energy demand, the diesel generator bridges the gap. An essential step before moving on to size is modeling the hybrid system. Each renewable energy source's power output and storage system are estimated via mathematical functions.

3.1.1. PV system model

Access to hourly solar radiation data is crucial for precisely planning hybrid systems. To accurately determine the power output of each photovoltaic panel in relation to the available solar radiation, equation (1) can be used [34]:

$$p_{PV}(t) = P_{R,PV} \times \left(R \,/\, R_{ref}\right) \times \left[1 + N_T\left(T_c - T_{ref}\right)\right] \quad (1)$$

where $p_{PV}(t)$ refers to the amount of power produced by each individual PV panel at a specific point in time, t. $P_{R,PV}$ is the rated power of the PV panel. The symbol "R" represents solar radiation and is based on the meteorological data of the site, which are measured in units of watts per square meter (W/m^2). The value "R_{ref}" represents the solar radiation under reference conditions and is typically standardized to 1000 W/m^2. T_{ref} is the cell's temperature under reference conditions typically set at 25 °C. The symbol "N_T" represents the photovoltaic panel's temperature coefficient, which is valued at -3.7×10^{-3} per degree Celsius (°C) [34]. This coefficient applies to both mono- and polycrystalline silicon types.

The cell temperature " T_c" can be determined via equation (2).

$$T_c = T_{\text{air}} + (((\text{NOCT} - 20) / 800) \times R_a) \tag{2}$$

where the variable T_{air} signifies the air temperature in the metrological data of the site, in degrees Celsius, while " R_a" represents radiation. Additionally, "NOCT" refers to the operating cell temperature measured in degrees Celsius. These specifications are crucial for photovoltaic (PV) modules and are officially provided by manufacturers. If the number of PV panels is denoted as N_{PV}, the generated power can be expressed as:

$$P_{\text{PV}}(t) = N_{\text{PV}} \times p_{\text{PV}}(t) \tag{3}$$

3.1.2. Wind turbine (WT) system model

Wind power is widely acknowledged as a promising form of energy. An advantage of this energy source is its lack of greenhouse gas emissions, rendering it environmentally sustainable. Moreover, wind power is economically efficient, further increasing its popularity. A wind turbine, consisting of multiple blades connected to a generator, is employed to capture and utilize wind energy. For energy capture, the turbine is placed on an elevated structure. The power output of each wind turbine can be determined via equation (4) [23,35]:

$$\begin{cases} \mathrm{P_{WT}(t) = 0} & \mathrm{V(t) < V_{IN}} \\ \mathrm{P_{WT}(t) = a(V(t))^3 - bP_R} & \mathrm{V_{IN} < V(t) < V_R} \\ \mathrm{P_{WT}(t) = P_R} & \mathrm{V_R < V(t) < V_{UP}} \\ \mathrm{P_{WT}(t) = 0} & \mathrm{V(t) > V_{UP}} \end{cases} \tag{4}$$

The parameters "a" and "b" are determined via equation (5).

$$\begin{cases} a = \dfrac{P_{R,\text{WT}}}{V_R^3 - V_{\text{IN}}^3} \\ b = \dfrac{V_{\text{IN}}^3}{V_R^3 - V_{\text{IN}}^3} \end{cases} \tag{5}$$

The total generated power can be denoted as:

$$P_{R,\text{WT}} = \frac{1}{2} A_{WT} \cdot C_P \cdot \rho_a \cdot \eta_{WT} \cdot V_R^3 \tag{6}$$

where the variable P_{WT} represents the generated power output of individual wind turbines at a given time point, the nominal power of a wind turbine is represented by the variable $P_{R,\text{WT}}$, and the wind speed is denoted by the variable "V", which is obtained from the metrological data of the site. The variable V_{IN} represents the speed at which the low cut occurs, whereas V_{UP} represents the speed at which the upper cut occurs. Additionally, V_R denotes the speed associated with the nominal power, which is based on the utilized wind turbine. The swept area of the wind turbines is shown as A_{WT}, and η_{WT} is the efficiency of the WT. The power coefficient, denoted as C_P, and the air density, represented by ρ_a.

3.1.3. Battery model

The battery's state of charge (SOC) can be represented on the basis of the time consumed. During the charging mode, the SOC can be expressed as [21]:

$$SOC(t) = SOC(t-1) \cdot (1 - \sigma) + E_{CH}(t) \tag{7}$$

where

$$E_{CH}(t) = ((P_{WT}(t) - P_L(t)) \times \eta_{inv} + P_{PV}(t)) \times \Delta t \times \eta_{CH} \tag{8}$$

In the discharge mode, the SOC can be expressed in the following form:

$$SOC(t) = SOC(t-1) \cdot (1 - \sigma) - E_{DIS}(t) \tag{9}$$

where

$$E_{DIS}(t) = \left(\frac{P_L(t) - P_{WT}(t)}{\eta_{inv}} - P_{PV}(t) \right) \times \Delta t \Big/ \eta_{DIS} \tag{10}$$

The symbol denotes the efficiency of an inverter η_{inv}. The variable σ represents the rate at which self-discharge occurs each hour. $E_{CH}(t)$, $E_{DIS}(t)$, and $P_{\text{load}}(t)$ are the charging energy, discharging energy, and load demand for energy at time t, respectively. The discharging and charging efficiencies for the storage system are denoted as η_{dis} and η_{ch}, respectively.

3.1.4. DG modeling

The DG supplies energy in the hybrid system when the PV, WT, and BESS cannot meet the load demands. DG fuel consumption may be computed as follows [36].

$$\mathrm{C}_{f\_DG}(\mathrm{t}) = \alpha_{DG} \times P_{DG}(t) + \beta_{DG} \times P_{rated\_DG} \tag{11}$$

The fuel consumption is denoted as C_{f_DG} (L/h). $P_{DG}(t)$ (kW) represents the average power. where P_{rated_DG} (kW) denotes the rated power of the DG. The consumption coefficient curve of the DG is given by the symbols α_{DG} and β_{DG}, with corresponding values of 0.246 L/kWh and 0.08145 L/kWh [21].

The calculation of the yearly fuel cost C_{DG} needed to operate the generator throughout the system's lifespan is outlined as follows:

$$C_{DG} = C_F \times \sum_{t=1}^{8760} \mathrm{C}_{f\_DG}(t), \tag{12}$$

where *CF* is the unit fuel cost, set in this study at 0.8 USD/ Liter [21].

3.1.5. Life cycle cost (LCC)

The cost studies of the hybrid wind turbine/photovoltaic/battery (WT/PV/BESS), wind turbine/battery/photovoltaic/diesel (WT/BESS/PV/DG), and photovoltaic/battery (PV/BESS) schemes apply the concept of life cycle cost (LCC), which may be expressed as [37].

$$LCC = \sum_{m \in WT,PV,DG,BAT} (AC_m + AM_m + \mathrm{AREP}_m) + C_{DG}|_{for\ DG\ if\ any} \tag{13}$$

where the variables *AM*, *AC* and *AREP* denote the yearly maintenance, capital, and replacement costs, respectively.

3.1.6. LCC of PV panels

The capital and annual maintenance costs associated with solar panels are expressed as follows [37]:

$$AC_{PV} = N_{PV} \cdot C_{PV} \cdot \frac{i_r \cdot (1 + i_r)^{n_{PV}}}{(1 + i_r)^{n_{PV}} - 1} \tag{14}$$

$$AM_{PV} = N_{PV} \cdot C_{Mnt-PV} \cdot t_{PV} \tag{15}$$

The variables C_{Mnt-PV} represent the yearly maintenance cost. C_{PV} denotes the unit cost of each solar panel. N_{PV} is the number of PVs. Moreover, t_{PV} is the operating time of the PV. n_{PV} is the lifetime of the PV, and i_r denotes the interest rate.

3.1.7. LCC of WTs

The formulation for the maintenance (AC_{WT}) and capital cost (AM_{WT}) of wind turbines is as follows [37].

$$AC_{WT} = N_{WT} \cdot C_{WT} \cdot \frac{i_r \cdot (1 + i_r)^{n_{WT}}}{(1 + i_r)^{n_{WT}} - 1} \tag{16}$$

$$AM_{WT} = N_{WT} \cdot C_{Mnt-WT} \cdot t_{WT} \tag{17}$$

The variables N_{WT}, C_{WT}, and C_{Mnt-WT} represent the number of wind turbine blades, the unit cost, and the yearly maintenance cost of each wind turbine, respectively. The variables n_{WT} denote the life of the WT, and t_{WT} is the operating time of the WT.

3.1.8. LCC of batteries

The financial expenses associated with the storage system, including

both the initial capital cost and the ongoing annual maintenance cost, can be mathematically represented as [37]:

$$AC_{BAT} = N_{BAT} \cdot C_{BAT} \cdot \frac{i_r \cdot (1+i_r)^{n_{BAT}}}{(1+i_r)^{n_{BAT}} - 1} \tag{18}$$

$$AM_{BAT} = N_{BAT} \cdot C_{Mnt-BAT} \cdot t_{batt} \tag{19}$$

In this context, N_{BAT} denotes the number of batteries, $C_{Mnt-BAT}$ refers to the yearly maintenance cost, and C_{BAT} represents the unit initial cost per battery. Moreover, t_{batt} represents the operating time of the battery. n_{BAT} signifies the life of the batteries.

3.1.9. LCC of the converter

The annual capital cost for the converter can be expressed as:

$$AC_{conv} = C_{cap\_conv} \cdot \frac{i_r \cdot (1+i_r)^{n_{conv}}}{(1+i_r)^{n_{conv}} - 1} \tag{20}$$

where (C_{cap_conv}) denotes the initial capital costs for the installation of the converter. n_{conv} signifies the life of the converter.

The operating and maintenance costs for the converter can be expressed as:

$$AM_{conv} = C_{O\&M\_conv} \cdot t_{conv} \tag{21}$$

where $C_{O\&M\_conv}$ denotes the operating and maintenance cost of the converter and where t_{conv} denotes the operating time of the converter.

3.1.10. LCC of DGs

$$AC_{DG} = N_{DG} \cdot C_{DG} \cdot \frac{i_r \cdot (1+i_r)^{n_{DG}}}{(1+i_r)^{n_{DG}} - 1} \tag{22}$$

$$AM_{DG} = N_{DG} \cdot C_{Mnt-DG} \tag{23}$$

The variables C_{Mnt-DG}, C_{DG}, and N_{DG} represent the yearly maintenance cost, the unit cost of each diesel generator, and the number of DG schemes, respectively [21]. n_{DG} signifies the life of the converter.

3.1.11. Replacement cost

Certain components of a photovoltaic/wind turbine/battery system necessitate replacement multiple times throughout the duration of the project's lifespan. The replacement cost of the hybrid system components throughout its lifetime is estimated as follows:

$$\mathrm{AREP} = \sum_{j=}^{n_{rep}} \mathrm{K}_{C\_rep} \mathrm{C}_u \left(\frac{1+i}{1+r}\right)^{nj/(n_{rep}+1)} \tag{24}$$

In this equation, i represents the inflation rate for replacements, K_{C_rep} is the capacity of the units used in the system, C_u denotes the cost of the replaced units, and n_{rep} refers to the number of replacements required over the project lifetime n. This study assumes that a battery's lifespan is five years [38]. Similarly, the converter/inverter is expected to have a lifespan of 10 years [37].

3.1.12. Net present cost

The total AC of the system, including all its components, can be expressed as [31].

$$AC = \left[N_{PV} \cdot C_{PV} \cdot \frac{i_r \cdot (1+i_r)^{n_{PV}}}{(1+i_r)^{n_{PV}} - 1} + N_{WT} \cdot C_{WT} \cdot \frac{i_r \cdot (1+i_r)^{n_{WT}}}{(1+i_r)^{n_{WT}} - 1} + N_{BAT} \cdot C_{BAT} \cdot \frac{i_r \cdot (1+i_r)^{n_{BAT}}}{(1+i_r)^{n_{BAT}} - 1} + C_{cap\_conv} \cdot \frac{i_r \cdot (1+i_r)^{n_{conv}}}{(1+i_r)^{n_{conv}} - 1} + N_{DG} \cdot C_{DG} \cdot \frac{i_r \cdot (1+i_r)^{n_{DG}}}{(1+i_r)^{n_{DG}} - 1} \right] \tag{25}$$

The following equation is utilized to calculate the annual maintenance cost considering the system components:

$$AM = N_{\mathrm{PV}} \times C_{Mnt-PV} \times t_{PV} + N_{\mathrm{WT}} \times C_{Mnt-WT} \times t_{WT} + N_{BAT} \cdot C_{Mnt-BAT} \times t_{batt} + C_{\mathrm{O\&M\_conv}} \times t_{conv} + N_{DG} \times C_{Mnt-DG} \times t_{DG} \tag{26}$$

The net present cost (NPC) of the system can be determined by:

$$NPC = \frac{LCC}{CRF} \tag{27}$$

where the total $LCC = AC + AM + \mathrm{AREP} + C_{DG}$ and the capital recovery factor (CRF) can be assumed to adapt the initial investment cost into an annual capital expense. It is calculated as $CRF(r,n) = \frac{r(1+r)^n}{(1+r)^n - 1}$. Moreover, r represents the interest rate (%), and n denotes the lifespan of the project under consideration.

3.2. Objective function and constraints

The objective function has been implemented to achieve the customer's required loss of power supply probability (LPSP) with a minimum levelized cost of energy (LCOE) and dummy load (P_{dummy}). It can be described as follows:

$$min\, f = \quad min\left(\lambda_1 LCOE + \lambda_2 LPSP + \lambda_3 P_{dummy}\right) \tag{28}$$

The chosen weighting factors are based on the relative significance of each objective variable, including LCOE, LPSP, and Pdummy. As a result, the objective function is adjusted using these weighting factors to minimize each objective, ultimately enhancing the overall operational performance. Determining the most suitable values for λ_1, λ_2, and λ_3 requires a trial-and-error approach to obtain the most favorable results. To be crucial, the aggregate of these weighting factors must equal 1. The values allocated to λ_1, λ_2, and λ_3 in this investigation are 0.4, 0.5999, and 0.0001, respectively.

The identified constraints are as follows:

$$N_{\mathrm{WT}} \geq 0 \tag{29}$$

$$N_{\mathrm{PV}} \geq 0 \tag{30}$$

$$N_{DG} \geq 0 \tag{31}$$

$$N_{BAT} \geq 0 \tag{32}$$

$$P_{WT}(t) + P_{PV}(t) + P_{BAT} + P_{DG}(t) \geq P_L(t) \tag{33}$$

$$LPSP_{Desired} \geq LPSP \tag{34}$$

$$SOC_{max} \geq SOC(t) \tag{35}$$

$$SOC_{\min} \leq SOC(t) \tag{36}$$

In this context, $\mathrm{SOC}_{\max}$ and $\mathrm{SOC}_{\min}$ represent the upper and lower bounds of the state of charge, respectively. One could compose written content.

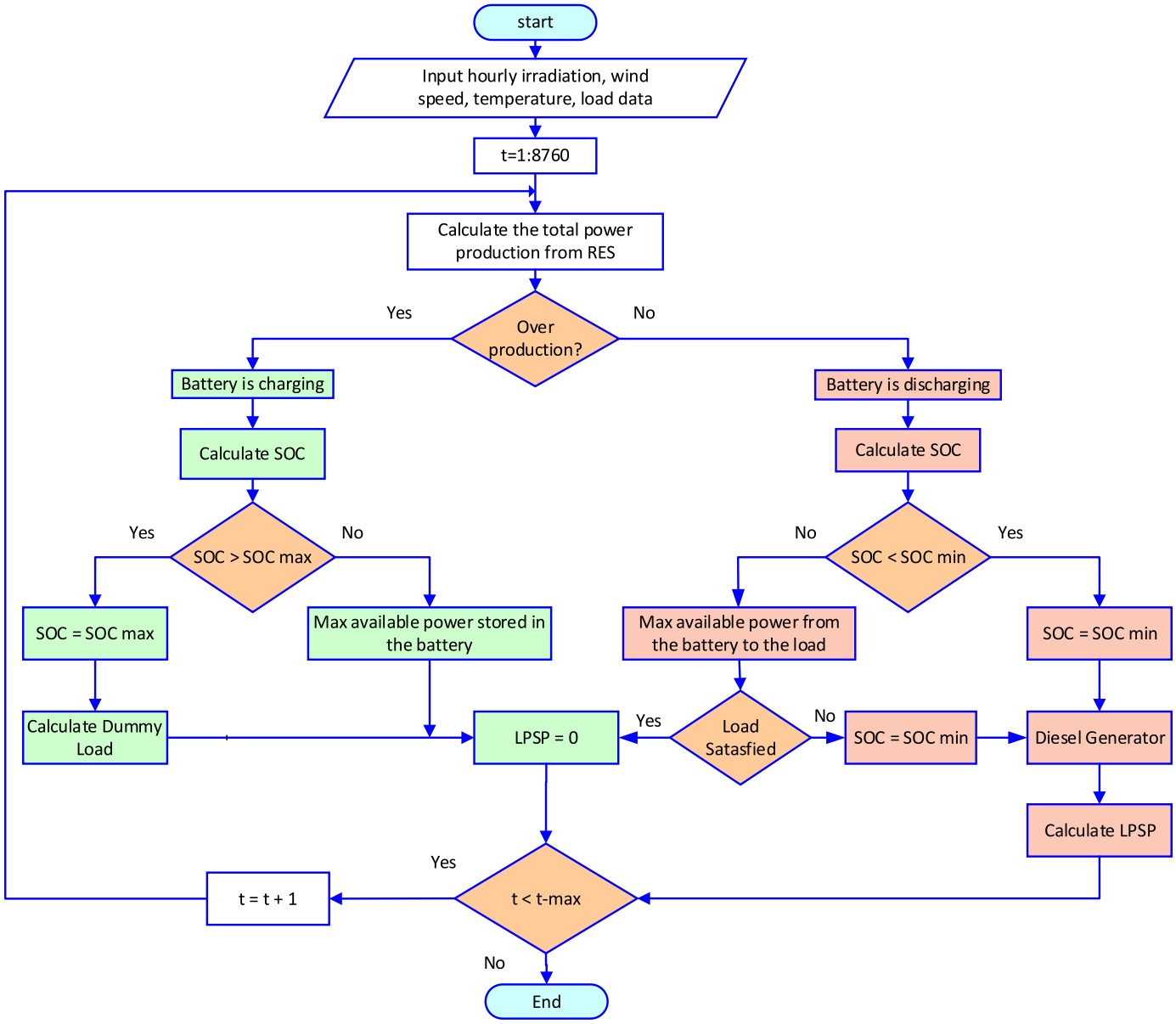

Fig. 3. Annual hourly operation plan of the hybrid MG.

$$SOC_{\min} = S_{BAT}(1 - DOD) \tag{37}$$

where DOD represents the maximum depth of discharge. S_{BAT} denotes the nominal capacity of the storage system. In the following subsections, the mathematical expressions of the objective function component and associated constraint are introduced.

3.2.1. Loss of power supply

When the state of charge at time t, denoted as SOC(t), falls below the minimum state of the charge threshold ($SOC_{\min}$), the storage system fails to meet part of the load. Afterward, when the state of charge ($SOC_{\min}$) at time t is equal to the minimum SOC ($SOC_{\min}$), the loss of power supply (LPS) can be expressed in the following form:

$$LPS(t) = P_L(t) \times \Delta t - (P_{DG}(t) + P_{WT}(t)) \times \Delta t - ((P_{PV}(t) \times \Delta t) + SOC(t - \Delta t) - SOC_{min}) \times \eta_{conv} \tag{38}$$

To provide a high level of reliability, it is imperative to consider the possibility of power supply loss (referred to as LPSP) while implementing hybrid renewable energy systems. The loss of power supply probability (LPSP) is a parameter measured on a scale from 0 to 1. A value of LPSP = 0 indicates that the load is consistently satisfied, whereas a value of LPSP = 1 indicates that the load is never satisfied. The power reliability needs to change on the basis of the load characteristics of different systems. According to Ref. [39], the $_{LPSPD}$, which represents the maximum allowed level of low-power supply probability (LPSP), is estimated to be approximately 0.02 in the context of rural and standalone applications. In this study, it is assumed that the LPSPD value is 0.02. This means that a reliability constraint of LPSP <0.02 is implemented in the optimization of the power generation system. The calculation of the LPSP can be performed for a specific time, denoted as T, via the following formula [33]:

$$LPSP = \frac{\sum_{t=1}^{T} LPS(t)}{\sum_{t=1}^{T} E_{Load}(t)} \tag{39}$$

The variables DOD, $S_{BAT,}$ P_{PV}, P_{WT}, P_{BAT}, $P_{DG,}$ and P_L represent the maximum depth of discharge, nominal capacity of the storage system,

solar power, wind power, battery power, diesel generator power, and load power, respectively.

3.2.2. Calculation of the dummy load

Occasionally, when the battery reaches its maximum capacity while renewable energy exceeds demand, the surplus energy is directed to a dummy load. This interval, during which the dummy load is activated, is denoted as:

$$P_{dummy}(t) \times \Delta t = (P_{WT}(t) - P_{load}(t)) \times \Delta t + (P_{PV}(t) \times \Delta t - E_{CH}(t)) \times \eta_{conv} \tag{40}$$

It can be represented as follows in another expression:

$$E_{dummy}(t) = E_{CH}(t) - (E_{bmax} - E_b(t)), if\ E_b(t) = E_{bmax} \tag{41}$$

$$E_{dummy}(t) = 0, if\ E\_b(t) < E\_\{bmax\} \tag{42}$$

where $E_{dummy}(t) = P_{dummy}(t) \times \Delta t$ is the excess energy.

3.2.3. Renewable energy fraction

The renewable energy fraction R_f is determined by dividing the total renewable energy by the total annual consumed energy as follows:

$$R_f = \frac{E_{ren}}{E_{tot}} \tag{43}$$

where E_{ren} is the total renewable energy (kWh) and where E_{tot} denotes the total annual energy consumption (kWh).

3.2.4. CO2 emissions

The total amount of CO2 emissions can be calculated as follows:

$$Q_{co2}(kgCO2/year) = \quad TotalC_{f_{DG}}(litre/year) \times EmissionFactor(kgCO2/litre) \tag{44}$$

In this context, Q_{CO} denotes the total CO_2 emission amount ($kgCO2\ /year$), TotalC_{f_DG} represents the total yearly fuel consumption ($litre\ /year$), and EF represents the emission factor for the fuel used (kgCO2 /litre). For the diesel fuel analyzed in this study, the default CO2 emission factor is 2.6533 (kgCO2 /litre).

3.2.5. Levelized cost of energy (LCOE)

The levelized cost of energy (LCOE) is a crucial quantity in economic systems. It quantifies the average unit cost of generating useable power within a given scheme. Mathematically [31], can be expressed as,

$$LCOE = \frac{\text{LCC}}{\sum_{t=1}^{8760} \text{P}_\text{L}(\text{t})} = \frac{\text{Total Life Cycle Cost}}{\text{Total Lifetime Energy Production}}. \tag{45}$$

3.3. Energy flow scenarios

The energy management system strategy within the designed microgrid is implemented to guarantee an uninterrupted energy supply to meet the demand. This energy management process encompasses four distinct scenarios. Fig. 3 shows the operational approach utilized by the independent hybrid power systems each hour throughout the year. Moreover, the energy flow scenarios can be described as follows.

3.3.1. Charging mode

3.3.1.1. Scenario A. Conversely, in cases where the energy generated from renewables surpasses the load demand, the battery is utilized in charging mode.

3.3.1.2. Scenario B. When the state of charge (SOC) of the battery reaches its maximum level and surplus electricity is available, the excess electricity is directed to a dummy load.

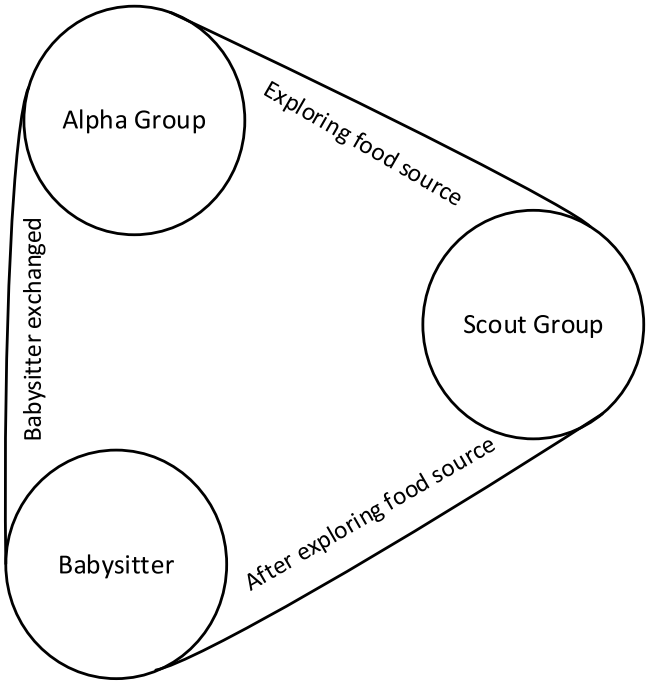

Fig. 4. The optimization steps of the indicated DMOA.

3.3.2. Discharging mode

3.3.2.1. Scenario C. If the generated electricity falls short of the load requirement, the BESS can be discharged to fulfill the demand. If the battery discharge is insufficient, a diesel generator is incorporated into the system as a backup.

3.3.2.2. Scenario D. If the renewable energy, battery, and DG fail to meet the load requirements consistently, resulting in an energy shortage, the load power loss (LPS) should be minimized through calculation.

3.4. The DMOA model

The DMOA algorithm under consideration imitates the compensatory behavioral adjustments observed in dwarf mongooses, including constraints related to prey size, social structure, and a seminomadic lifestyle. The social structures are categorized into alpha, scout, and babysitter groups, facilitating migratory tendencies and territorial exploration. The proposed DMOA method is delineated in three distinct phases, as depicted in Fig. 4. The equations presented below are sourced from Ref. [40] (see Fig. 5).

3.4.1. Population initialization

As shown in Eq. (46), the DMOA optimization starts by setting up the possible population of mongooses X. The population is made randomly among the upper bound UB and lower bound LB of the prearranged situation.

$$X = \begin{bmatrix} x_{1,1}\ x_{1,2} \cdots x_{1,d-1}\ x_{1,d} \\ x_{2,1}\ x_{2,2} \cdots x_{2,d-1}\ x_{2,d} \\ \vdots\ \vdots x_{i,j} \vdots\ \vdots \\ x_{n,1}\ x_{n,2} \cdots x_{n,d-1}\ x_{n,d} \end{bmatrix} \tag{46}$$

The set of current candidate populations, denoted as X, is produced randomly via Equation (47). where $x_{i,j}$ represents the spatial location of the jth dimension within the ith population. The value of n describes the

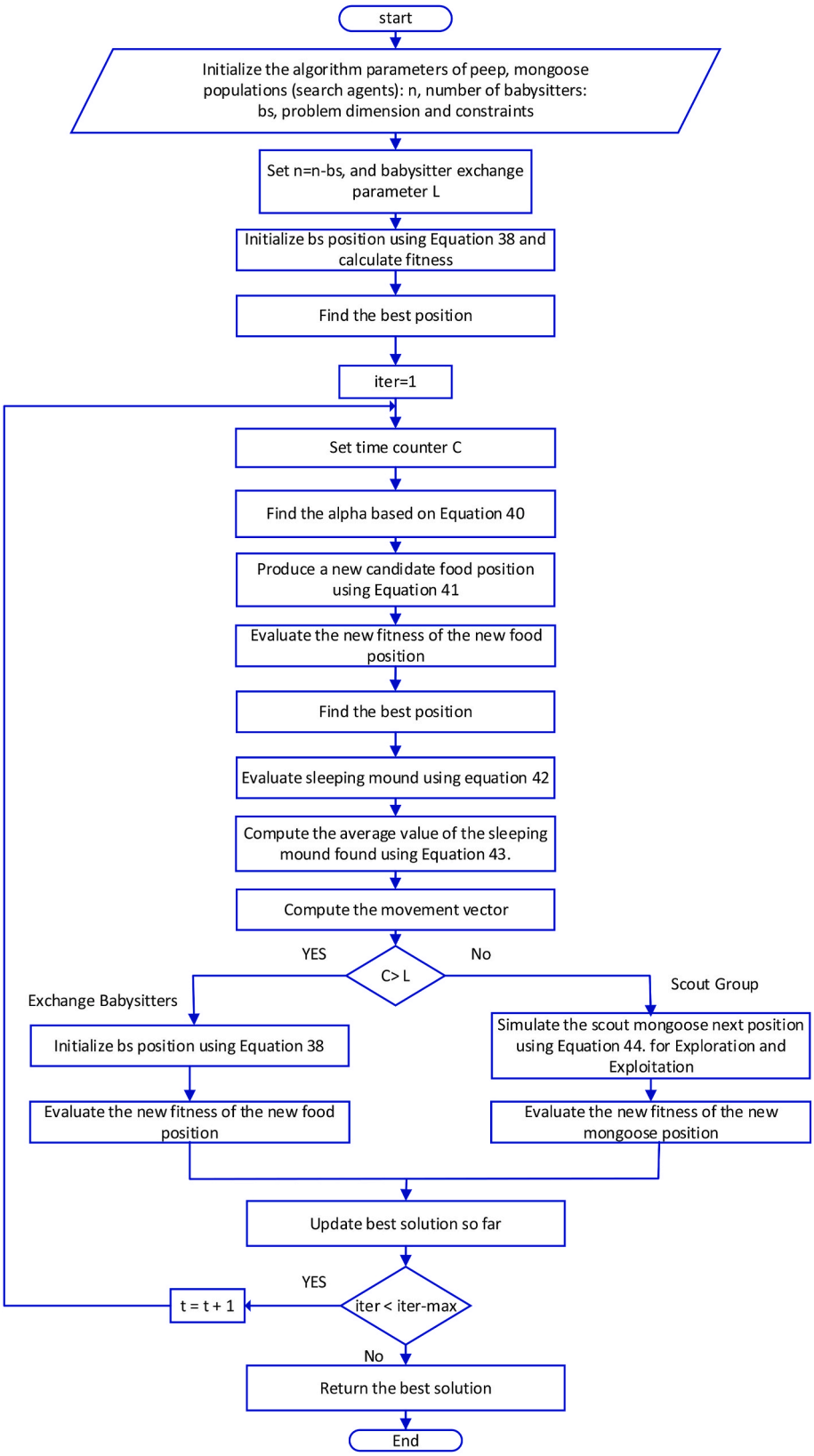

Fig. 5. Flow Chart of DMOA.

size of the population, whereas d defines the dimension of the problem.

$$x_{i,j} = unifrnd(Var_{Min}, Var_{Max}, Var_{Size}) \quad (47)$$

The function *unifrnd* generates a random number that follows a uniform distribution. Var_{Min} and Var_{Max} refer to the lower and upper bounds of the problem, respectively. The variable Var_{Size} represents the size of the choice variables or the dimensions of the problem.

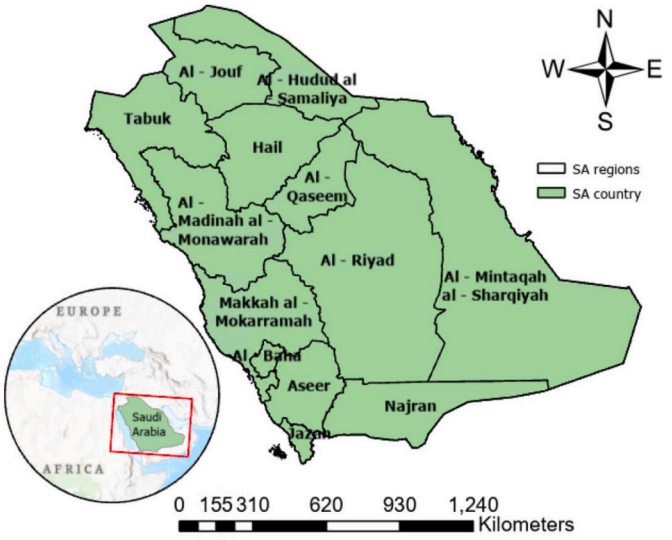

Fig. 6. Location of the study area (Najran, situated in southern Saudi Arabia) [43].

3.4.2. Alpha group

After the initialization of the population, the fitness of each solution is calculated. The probability value for the fitness of each population is determined via Equation (44), and the selection of the alpha female, α, is based on this probability.

$$\alpha = \frac{fit_i}{\sum_{i=1}^{n} fit_i} \tag{48}$$

The quantity of mongooses within the alpha group is proportional to the value denoted as $n - bs$. In addition, bs is the variable denoting the quantity of babysitters. The vocalization emitted by the alpha female, known as a *peep*, serves as a means of guiding and maintaining cohesion within the family unit.

Each mongoose sleeps in the first sleeping mound, which is set to 0. The DMOA uses the expression in equation (49) to create a possible food spot.

$$X_{i+1} = X_i + phi^{*}peep \tag{49}$$

where *phi* is a random number that is spread out evenly between −1 and 1. The sleeping mound is given in equation (50) after each repetition.

$$sm_i = \frac{fit_{i+1} - fit_i}{\max\{|fit_{i+1}, fit_i|\}} \tag{50}$$

Equation (51) provides the mean value of the discovered sleeping mound.

$$\varphi = \frac{\sum_{i=1}^{n} sm_i}{n} \tag{51}$$

The variable n represents the number of Babysitters.

3.4.3. Scout group

The scouts aim to identify new sleeping mounds, as mongooses tend to avoid revisiting previously utilized mounds, promoting a continuous exploration process. The scouting is conducted concurrently with foraging, wherein the total efficacy of locating a new mound is assessed. According to the model, the family might encounter a previously unidentified mound by venturing a sufficient distance during foraging activities. The scout mongoose is simulated via equation (52).

$$X_{i+1} = \begin{cases} X_i - CF * phi * rand * \left[X_i - \vec{M}\right] & if \varphi_{i+1} > \varphi_i \\ X_i + CF * phi * rand * \left[X_i - \vec{M}\right] & else \end{cases} \tag{52}$$

where rand denotes a random variable $[0, 1]$.

$CF = \left(1 - \frac{iter}{Max_{iter}}\right)^{\left(2\frac{iter}{Max_{iter}}\right)}$" is used to regulate the collective-volitive movement of the group of mongooses, and it is progressively reduced in a linear manner as the number of iterations increases. The vector $\vec{M} = \sum_{i=1}^{n} \frac{X_i \times sm_i}{X_i}$ represents the directional movement of the mongoose toward the new sleeping mound.

3.4.4. The babysitters

The technique entails implementing a rotation system for babysitters, enabling the alpha female to assume leadership during the group's daily foraging activities. The quantity of Babysitters is contingent upon the magnitude of the population and influences the algorithm through a decrease in the overall population size. The algorithm emulates the behavior of this group by decreasing the population size on the basis of the fraction that represents Babysitters. The babysitter exchange parameter resets the scouting and food source data while assigning a fitness weight of zero to the babysitters. The decrease in the mean weight of the alpha group throughout subsequent iterations impedes the collective mobility of the group and accentuates the focus on exploitation.

4. Simulation results and discussion

4.1. Research region and data selection

The city of Najran, situated in southern Saudi Arabia, holds historical significance because of its role as a crucial junction connecting the northern, western, and Yemeni regions, as shown in Fig. 6. Geographically, Najran is positioned between 17 and 20° north latitude and 44 and 52° east longitude. Its climate is characterized by dry winters and a humid-subtropical climate, designated "CWa" according to the Köppen–Geiger classification system [41].

This research investigated the performance and economic feasibility of a hybrid system on the basis of the actual weather conditions of Najran. Najran is renowned for being one of the most contemporary cities. The Najran region had a population of 569,000 people in 2014, accounting for 1.85 % of the total population of the Kingdom, which was 30.8 million [42].

The data for this location were analyzed continuously for 8760 h. The data indicate that the area under investigation experiences consistently high levels of solar radiation and high wind speeds throughout the year. Moreover, the examined region is highly conducive to establishing both photovoltaic (PV) and wind power plants. Therefore, it holds significant promise for the implementation of PV facilities.

Fig. 7 displays a wind speed map of Saudi Arabia, highlighting that the prevailing wind speeds across most of the country typically fall within the range of 5–8 meters per second (m/s), making them well suited for wind energy generation via turbines. The selected study sites are characterized by wind speeds ranging from 4.28 to 7.21 m/s.

The annual fluctuations in the solar radiation intensity and wind speed are visually represented in Fig. 8. On the basis of the available data, the mean daily solar radiation is 227.08 kWh/m^2 on average, whereas the typical wind speed is 6.890 m/s. Notably, the average power demand in this area is 260 kW.

The power demand in kW for a specific day is demonstrated in Fig. 9. The peak power is 375 and 340 kW in summer and winter, respectively. Table 2 lists the system components (PV, WT, DG, and BESS) and their characteristics.

This study assumes a system lifetime of 25 years and a 6 % interest

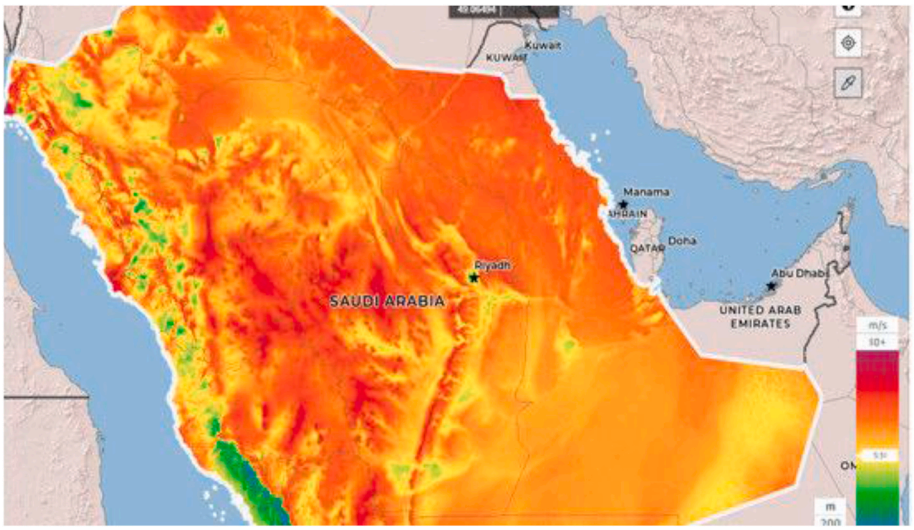

(a)

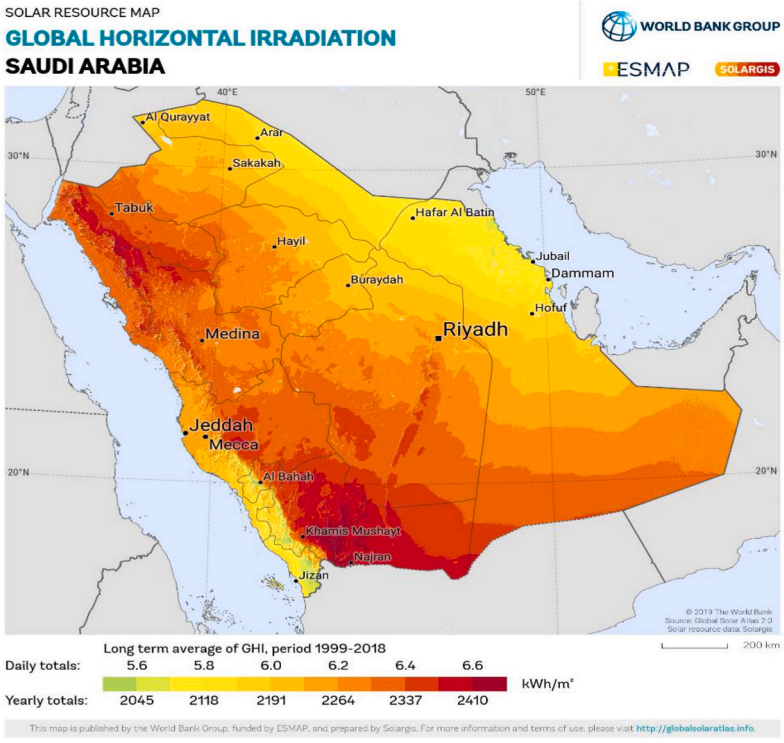

(b)

Fig. 7. (a) Wind speed map in Saudi Arabia. (b) Solar radiation intensity in Saudi Arabia [44].

rate. Simulation programs such as MATLAB for optimization have been used to analyze the results. The number of iterations and number of search agents are set to 60 and 20, respectively, in the optimization algorithms. The parameter values of the tested algorithms are as follows: for the WOA, the value of α decreases from 2 to 0, and the value of b equals 2 [45]. The DMOA has only one parameter, CF, that can be tuned via $CF = \left(1 - \frac{iter}{Max_{iter}}\right)^{\left(2*\frac{iter}{Max_{iter}}\right)}$. For SSA [46], the parameters are only the number of slaps and the maximum number of iterations.

4.2. Results and simulations of the optimal case

The optimal number of PV modules, WTs, battery banks, and DGs that produce the desired output constitute the optimal capacity of a hybrid system. The outcomes of the optimization procedure are shown in Table 3. Moreover, Fig. 10 illustrates the best result of the objective function over the iterations. The DMOA algorithm achieves an optimum value of 0.220724271 within the predefined operational limits after 10 iterations. In contrast, the SSA algorithm achieves an optimum value of 0.225137323 within the predefined operating limits after 40 iterations. The WOA achieves an optimum value of 0.229935171 after 30

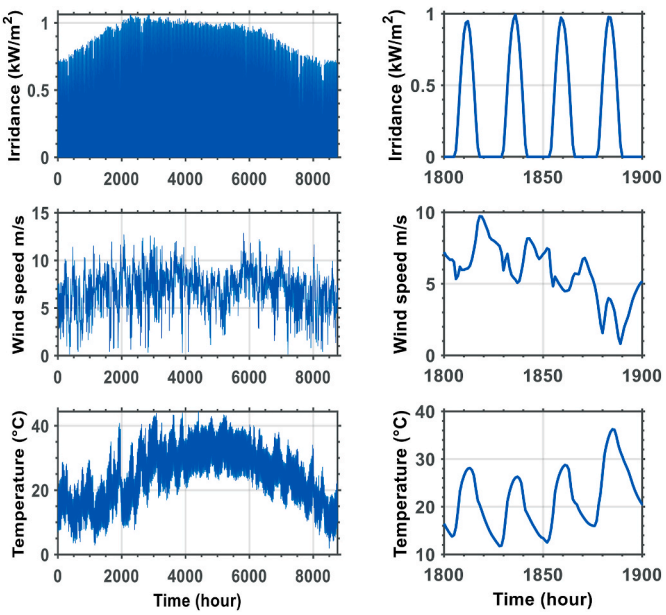

Fig. 8. Hourly solar radiation and wind speed in the study area.

iterations, as illustrated in Fig. 10. Fig. 11 displays the specific expenses of the system components considering the net present value of each component and their summation, which provides the LCC.

More investigations have been conducted to evaluate the three applied optimization algorithms. The renewable energy fraction has been calculated, and its value is 0.7429 for the three algorithms, whereas the CO2 emissions (tonCO2/year) are 714.69, which is less than those obtained with the application of the SSA and WOA.

4.3. Robustness of the applied algorithms

The robustness of the WOA, SSA, and DMOA was demonstrated through thirty consecutive executions. Table 4 presents the statistical findings for these techniques on the basis of the recorded results. The data analysis included calculations of the standard deviation, minimum and maximum values, median values, and means from the ten runs. Table 4 also facilitates a comparison of the effectiveness of the WOA, SSA, and DMOA methods in minimizing the objective function. The table shows the RMSE and RE values, which shed light on how efficiently these techniques optimize the design of the RES. The simulation results demonstrate that the DMOA method outperforms the other methods in terms of the mean, median, maximum, standard deviation, relative error, mean absolute error, root mean square error, and efficiency. The formulas can be described as follows:

$$\text{Standard Deviation (SD)} = \sqrt{\frac{\sum_{k=0}^{n_{Run}} (X_i - X^-)}{n_{Run} - 1}} \tag{53}$$

$$\text{Root Mean Square Error (RMSE)} = \sqrt{\frac{\sum_{i=1}^{n_{Run}} (X_i - X_{min})^2}{n_{Run}}} \tag{54}$$

$$\text{Relative Error (RE)} = \frac{\sum_{i=1}^{n_{Run}} (X_i - X_{min})}{X_{min}} \tag{56}$$

$$\text{Mean Absolute Error (MAE)} = \frac{\sum_{i=1}^{n_{Run}} (X_i - X_{min})}{n_{Run}} \tag{57}$$

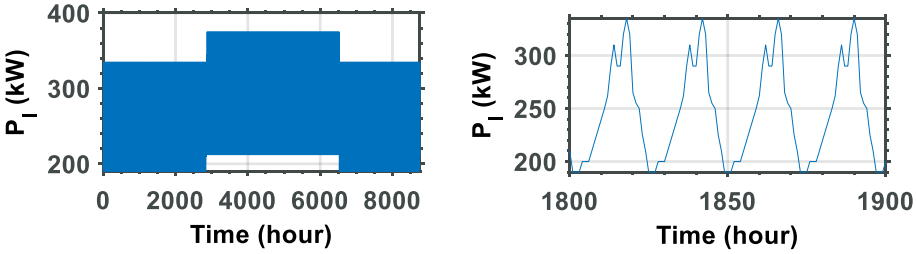

Fig. 9. Daily load demand curve.

Table 2
Characteristics of the system components.

Data of PV modules		**Data of wind turbine**		**Data of Battery Bank**	
Parameter	Value	Parameter	**Value**	Parameter	Value
Model	*PV − MLT260HC*	Model	*Fuhrländer FL* 30	*Model*	*RS lead − acid battery*
Max. power	260 *W*	Rated power	30 *kW*	*Size*	12*v*(50*Ah*)
Length	1625 *mm*	Rotor diameter	12.8 *m*	*Efficiency*	86 %
Width	1019 *mm*	Swept area	$13m^2$	*DOD*	0.8
Thickness	46 *mm*	Cut − in speed	$\frac{2.6m}{s}$	*Weight*	16.5 *kg*
Modules Efficiency	15.7%	Cut − off speed	$25\frac{m}{s}$	*Max. discharge current*	750 *A*
Operating temperature	47°*C*	Rated speed	$12.1\frac{m}{s}$	*Internal resistance*	<= .006 *Ω*
Temperature coefficient	0.45%	Initial cost	58565.79 *USD*	*Operating Temperature*	0 − 47°*C*
Initial cost	112 *USD*	Replacement cost	34563.226 *USD*	*Initial cost*	58564.79 *USD*
O&*M cost*	1%	O&*M cost*	2.99%	*O&M cost*	3%
Lifetime	25 *years*	Lifetime	20 *years*	*Replacement cost*	34553.226 *USD*
Data of diesel generator					
Rated power for one DG	100*kw*	*Replacement cost*	850 *USD*	*O&M cost*	3%
Initial cost	850 *USD*	*Lifetime*	10*Years*	Fuel Cost	0.8 *USD*/*litre*

Table 3
Results of the optimization methods.

	SSA	WOA	DMOA
Best objective function	0.225137323	0.229935171	0.220724271
LCOE(US$/kwh)	0.198683288	0.199357062	0.199096222
LPSP	6.51412E-09	3.07434E-07	3.20657E-09
n_PV	1100	1100	1100
n_WT	14	14	14
n_batt	307	229	400
n_DG	2	2	2
Dummy Load(kwh)	14.56	15.019	14.108
RF	0.7429	0.7429	0.7429
CO2 Emissions (tonCO2/year)	7252.6	7514.0	7146.9

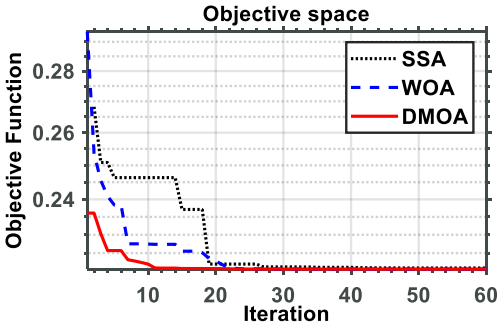

Fig. 10. Convergence curves of the optimization technique, demonstrating the best score obtained to date.

$$\text{Efficiency} = \frac{\sum_{i=1}^{n_{Run}} \left(\frac{X_{min}}{X_i}\right)}{n_{Run}} * 100\% \quad (58)$$

In this context, X_i represents the cost function for the applied technique in each iteration. X_{min} represents the optimal value obtained, whereas n_{Run} denotes the number of runs conducted via MATLAB software.

Fig. 12 shows the convergence characteristics of these ten runs. The uniformity of the curves depicted in Fig. 12 highlights the resilience of the DMOA technique. A comparison of the results of the DMOA with those of the WOA and SSA clearly reveals that the DMOA is significantly effective in parameter optimization. The DMOA outperformed the WOA in terms of both objective function values. Since most optimization algorithms draw inspiration from nature, tracking efficiency is gauged by how frequently the algorithm converges to the best solution. Specifically, the DMOA achieves the best objective function value of 0.220724269 and a tracking efficiency of 99.99 in 10 runs, outperforming the WOA with values of 0.22143995 and 95.33284247 for the least efficient algorithm. Furthermore, the top-performing algorithm demonstrates efficiencies nearing 100 %, reinforcing the suitability of the DMOA for optimizing the studied RE optimization problem.

The efficacy of the examined techniques was evaluated via a Wilcoxon signed-rank test, and the results are displayed in Table 5. The Wilcoxon signed-rank test revealed that the P values for the WOA, SSA, and DMOA are consistently 2×10^{-3}. All the evaluated methods yield a rank value of 1, which is consistent with the Wilcoxon signed-rank test. In addition, all of the methods under evaluation demonstrate statistical significance.

Fig. 13 presents the analysis of the results via boxplots from 10 executions, providing a comprehensive statistical illustration. The figure displays the outcomes of 10 runs, presenting the distribution of results across the boxplots. Significantly, the WOA, SSA, and DMOA methods consistently produce the most favorable values for the objective function throughout the ten runs.

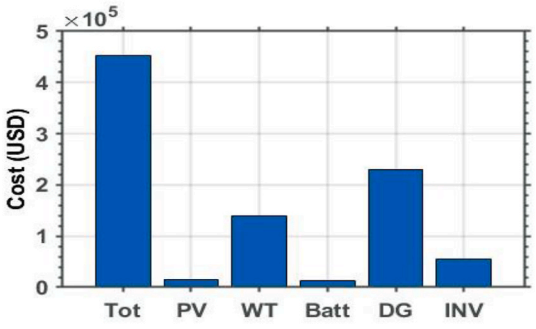

Fig. 11. Cost details of the system components.

Table 4
The statistical findings for these techniques are based on the recorded results.

Statistical Indices	SSA	WOA	DMOA
Min.	0.220726232	0.22143995	0.220724269
Max.	0.227897784	0.266192081	0.220724282
Mean	0.223670752	0.232827093	0.220724275
Median	0.222836652	0.229948466	0.220724273
SD	0.273371769	1.248740767	$4.85477E-07$
RE	0.133401449	0.514231616	$2.49265E-07$
MAE	0.00294452	0.011387142	$5.50188E-09$
RMSE	0.003923785	0.016431945	$7.17513E-09$
Eff.	98.69674515	95.33284247	99.99999751

4.4. Findings from the optimal sizing analysis

The research described in the paper utilized a comprehensive dataset and technoeconomic parameters as inputs for the model. The model then underwent 60 iterations of the DMOA. The process yields several optimal decision variables, minimizing critical metrics such as the NPC, COE, and LPSP. To facilitate a comparative analysis of different microgrid configurations under similar conditions, nine distinct combinations have been created, incorporating components such as DGs, PVs, WTs, and batteries, which are PV/WT/BESS, WT/BESS, PV/BESS, PV/WT PV/WT/BESS/DG, PV/BESS/DG, PV/WT/DG, WT/DG and PV/DG. The outcomes of these optimizations are presented in Tables 6 and 7.

Table 6 provides a comprehensive overview of various configurations, including PV/WT/BESS/DG, PV/BESS/DG, PV/WT/DG, WT/DG, and PV/DG. Among these, the PV/WT/BESS/DG configuration emerged as the most cost-effective choice, demonstrating its efficiency, with a remarkably low LCOE of 0.199 USD/kWh and a minimal LPSP of 1.9×10^{-8}%. This configuration has proven highly competitive despite its complexity, as evidenced by an NPC of 5,798,338 USD. In contrast, configurations such as PV/BESS/DG and PV/DG, while having lower LCOE, incurred significantly higher overall costs and initial investments. The table also shows the optimal size of each configuration.

Table 7 presents the results to clarify the impact of the absence of the DG from the configuration, which results in a greater value of LPSP, indicating the absence of system reliability in such cases. Moreover, the results validate the results of the suggested configuration of PV/Wind/DG/BESS. The analysis in Table 7, which excluded DG systems, highlighted the PV/WT/BESS configuration. It exhibited an adequate balance between efficiency and costs, with a moderate LCOE of 0.098 USD/kWh and an LPSP of 0.311 %. However, its high NPC of 2,851,666 USD indicated a substantial long-term investment. Comparatively, PV/BESSs stand out because of their exceptionally low LCOE, effectively managing both initial and long-term costs. However, the LPSP of the PV/BESS configuration is recorded as 0.679 in the table, indicating a lower level of reliability. The table also shows the optimal size of each configuration. In the results of Table 7, the LPSP is not constrained or evaluated as a part of the optimized objective function to show the DG impact in each configuration. Finally, the results show that the reliability of each

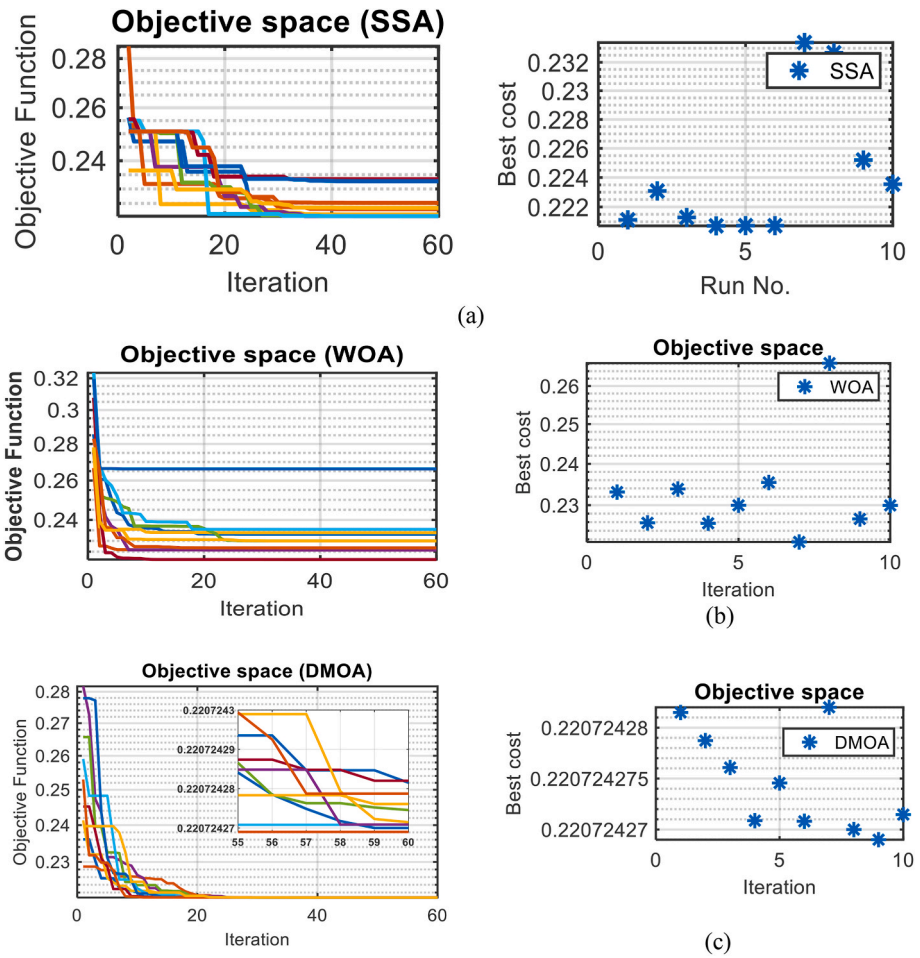

Fig. 12. Convergence curves for ten executions employing the (a) SSA, (b) WOA, and (c) DMOA.

Table 5
Wilcoxon signed rank test.

	SSA	WOA	DMOA
p value	2E-03	2E-03	2E-03
Rank	1	1	1

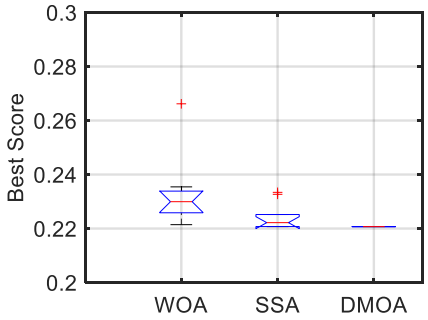

Fig. 13. Best results at the 30th run for the SSA, WOA, and DMOA.

configuration whose DGs are not present is poor compared with those of Table 6. Notably, the absence of the DG is also reflected in the decrease in the emission to zero.

4.5. Performance of the MG

Fig. 14 illustrates the hourly fluctuations in power generation for different elements within the suggested hybrid system under optimal DMOA conditions. The components depicted include the power demand (P_I), the total power generated from renewable sources, wind turbines, and photovoltaics (P_{WT}, P_{pv}, the power produced by diesel units (P_{DG}), the number of diesel generator units in operation each hour (DG_{unit}), the dummy load power (P_{dummy}), and the power involved in charging and discharging the storage battery system (P_{CH}&P_{DIS}). Additionally, it indicates the state of charge of the battery bank system as a percentage of its total capacity (SOC) and the fuel consumption of the diesel generator units. The discrepancy, denoted as P_{diff}, represents the contrast between the power demand P_I and the total power generated from renewable sources (P_{WT}, P_{pv}).

Figs. 15 and 16 depict the results of DMOA during distinct winter and summer timeframes, ranging from 1800:1823 h and from 4980:5003 h, presenting the results of one day in winter and another day in summer. The daily power load curve displays two clear peaks. The initial peak occurs at 13:00, during midday, at high temperatures. The second peak occurs at 17:00, following sunset, coinciding with the time when all consumers return to their residences. During the late night and early morning hours, the power produced by the PV array and WT is notably limited.

Therefore, the two proposed DG units operate collaboratively at elevated capacity to effectively satisfy the load demand. As sunrise, the power generated by renewable energy sources increases, enabling a single DG unit and renewable sources to meet the demand adequately.

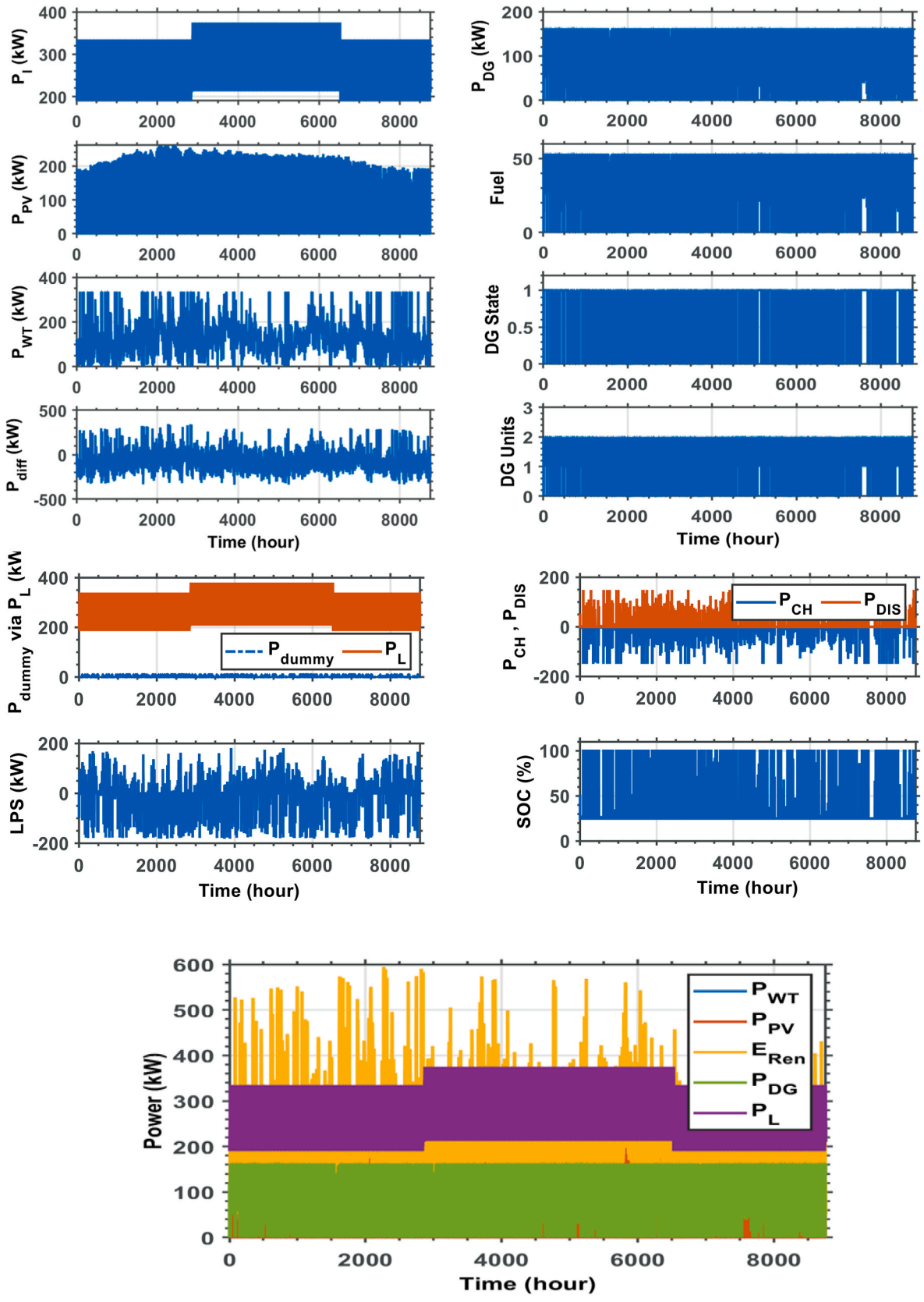

Fig. 14. Optimal sizing simulation results (DMOA, 8760 h).

Table 6
Comparative analysis of renewable energy configurations with DGs based on the DMOA.

Configurations Available technologies	Optimal configuration				LCOE (USD/kWh)	LPSP	NPC (USD)	CO_2 (tonCO2/year)	RF
	PV	WT	DG	BESS					
PV/WT/BESS/DG	1100	14	1.63	400	0.199	1.9 x 10-8	5798338	714.689	0.7429
PV/BESS/DG	1166.01	0	3.35	56.98	0.26	0.015	7456000	1728.599	0.2696
PV/WT/DG	1100	14	2.23	0	0.20	0.007	5893491	818.601	0.7429
WT/DG	0	14	2.61	0	0.23	0.005	6893054	1246.346	0.4886
PV/DG	1108.96	0	3.35	0	0.27	0.004	7841835	1751.2788	0.2564

Table 7
Comparative analysis of renewable energy configurations without DGs based on the DMOA.

Configurations Available technologies	Optimal configuration				LCOE USD/kWh)	LPSP (%)	NPC (USD)
	PV	WT	DG	BESS			
PV/WT/BESS	1100	14	0	400	0.098	0.3129	2850359.554
WT/BESS	0	18	0	1526	0.127	0.4030	3686035.825
PV/BESS	1421	0	0	564	0.041	0.6723	1181376.372
PV/WT	1100	14	0	0	0.085	0.3289	2467124.064

At noon, if the power generated by renewables exceeds the load demand, one DG unit is deactivated. The surplus energy is then used to charge the battery banks until they reach their maximum allowable limit, which is equivalent to a 100 % state of charge (SOC). When the battery reaches its maximum charge, surplus power is directed to a dummy load. In contrast, as the output from the hybrid renewable system decreases, the battery starts discharging energy until it reaches its minimum state of charge (SOCmin). At this stage, the DG unit recommends its operation.

4.6. Sensitivity analysis

Sensitivity analysis is a critical tool for understanding how variations in the number of renewable sources, specifically the number of PV panels and wind turbines, influence the overall performance of a smart grid system. By fixing the number of diesel generators and batteries at their optimal values, one can isolate the impact of renewable sources on key metrics such as total cost, cost of energy (COE), loss of power supply probability (LPSP), and the dummy load.

The results from the analysis indicate that increasing the number of PV panels and wind turbines from zero to meet the load demand tends to increase the total costs and COE to find the optimal variables, as shown in Fig. 17. However, while the total cost decreases with more renewable sources, the marginal benefit decreases after reaching a certain threshold, suggesting an optimal number beyond which additional investments yield falling returns. In terms of reliability, as the number of PV panels and wind turbines increases, the LPSP decreases significantly, reflecting increased energy availability and system resilience. In the context of the sensitivity analysis, the LPSP serves as a crucial indicator of system reliability. A value of 0 or lower indicates that the load is fully satisfied, meaning that the system can meet demand without any shortfalls. Conversely, a positive LPSP value indicates a failure to meet the load requirements, reflecting a shortage in the power supply. Moreover, the results show that the dummy load fluctuates on the basis of renewable output, further emphasizing the importance of integrating storage to manage variability. The analysis reveals the value of optimizing numerous renewable resources to achieve a balance between economic efficiency and system reliability.

More sensitivity analysis has been conducted to focus on examining the impact of varying the number of DGs while keeping the number of PV panels, WTs, and batteries at their optimal values. The analysis evaluates key metrics, including total annual cost, cost of energy (COE), reliability in terms of LPSP, fuel costs, power load ratios, renewable fraction (RF), and CO2 emissions.

The results are visualized in Fig. 18, which highlights the relationships between the number of DGs and the aforementioned parameters. For example, the analysis reveals how the cost, COE, and reliability change as the number of DG units varies. The red markers on the graphs indicate the optimal configurations of the PV, WT, DG, and battery systems, as derived from the optimization process. The analysis shows that increasing the number of DG installations generally leads to an increase in CO2 emissions and enhances system reliability, as shown in the graph of the LPSP. In addition, the renewable fraction (RF) is also constant because the system configuration should maximize the RES utilization. Increasing the number of DGs results in increased fuel costs and CO2 emissions. However, the total cost and COE are more sensitive to changes in the number of DGs, indicating their crucial role in the system's economic performance. These findings provide valuable insights into how different configurations of DGs and renewable energy sources affect the system's overall efficiency, cost effectiveness, and environmental impact.

4.7. Financial analysis

To thoroughly evaluate the proposed energy system configurations, it is crucial to extend the analysis beyond technical performance and explore financial metrics that assess the project's economic feasibility and long-term sustainability. The integration of renewable energy (RE) technologies and energy storage solutions involves substantial capital investment. Key financial metric, such as Payback Period (PBP), is vital for determining the financial viability of the RES.

As a result, the Discounted PBP for the optimal configured RES is 7.62 years, as shown in Fig. 19. Additionally, the total savings over 25 years amount to $5,241,406.72, while the total operating costs for the same period are $2,811,330.54. Moreover, the optimal configuration exhibits a Return on Investment (ROI) of 86.44 %, reflecting strong financial performance with a positive return. Additionally, it has an acceptable payback period, indicating a quicker return on investment. A positive ROI demonstrates that this configuration generates returns that exceed the initial investment.

4.8. Comparative analysis of the study results with those of previous studies

This section compares the study results with those of prior research on hybrid renewable energy systems. Several earlier studies are listed for analysis, utilizing the LCOE as a crucial metric. The LCOE measures the energy cost per kW and provides valuable insights into the potential of hybrid microgrid systems in diverse geographic conditions. Notably, the comparison does not focus on evaluating the quality of prior studies solely on the basis of LCOE. However, the objective is to provide energy

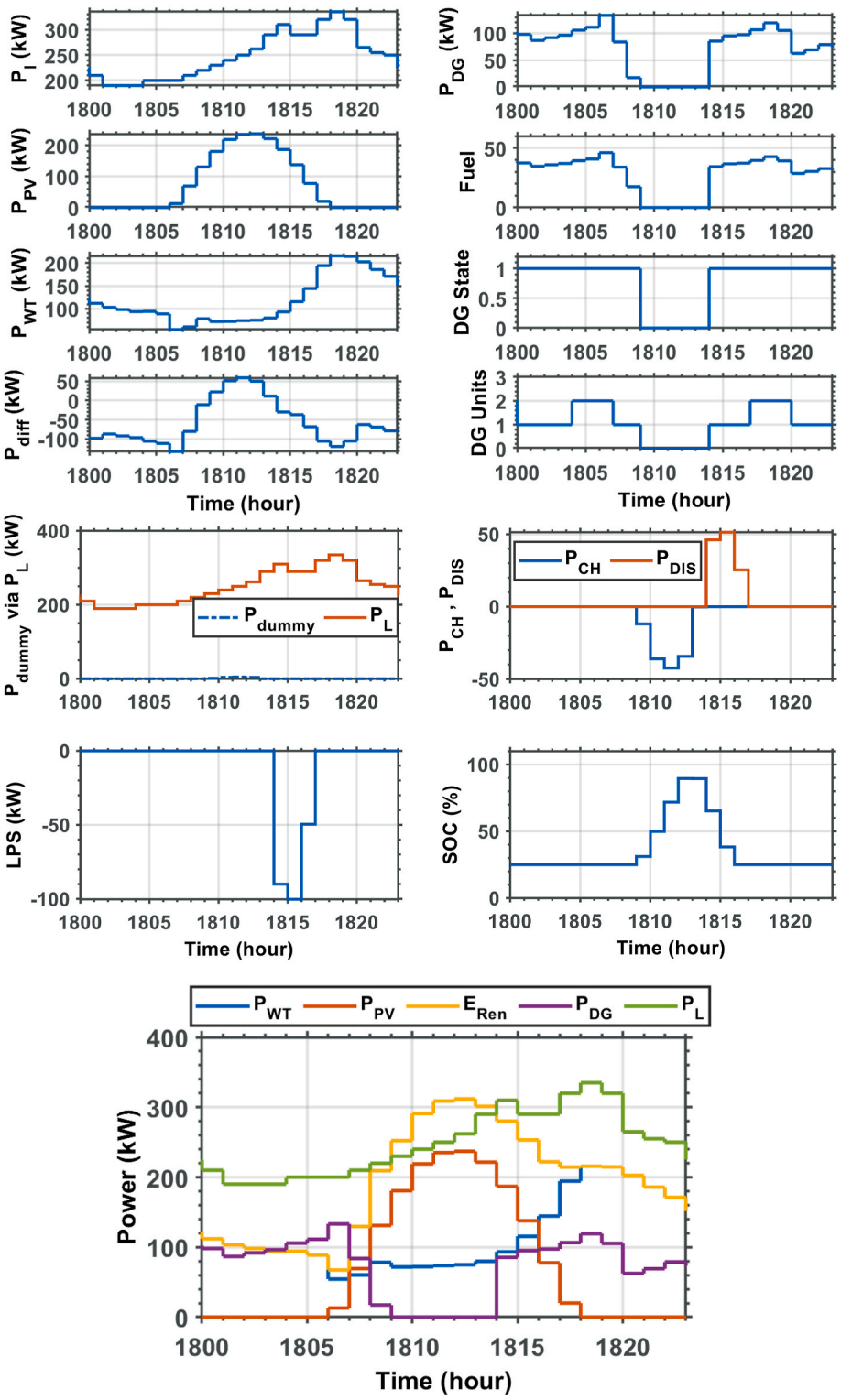

Fig. 15. The results of one day of simulation in March via DMOA.

system designers and organisations with insights into local renewable resources, using LCOE values as a reference.

Table 8 compares the proposed renewable-based microgrid system with those of previous studies. The analysis revealed that the hybrid system incorporating PVs, WTs, DGs, and batteries had the lowest LCOE among the configurations listed in previous studies. Nevertheless, the PV/BESS configuration has emerged as the most cost-effective scenario. Importantly, the first scenario, PV/WT/DG/BESS, was deemed more reliable on the basis of the earlier discussions presented in the study.

4.9. Recommendations

The PV/WT/BESS/DG microgrid configuration-based DOMA algorithm may be considered a recommended configuration on the basis of the introduced results and the following main reasons.

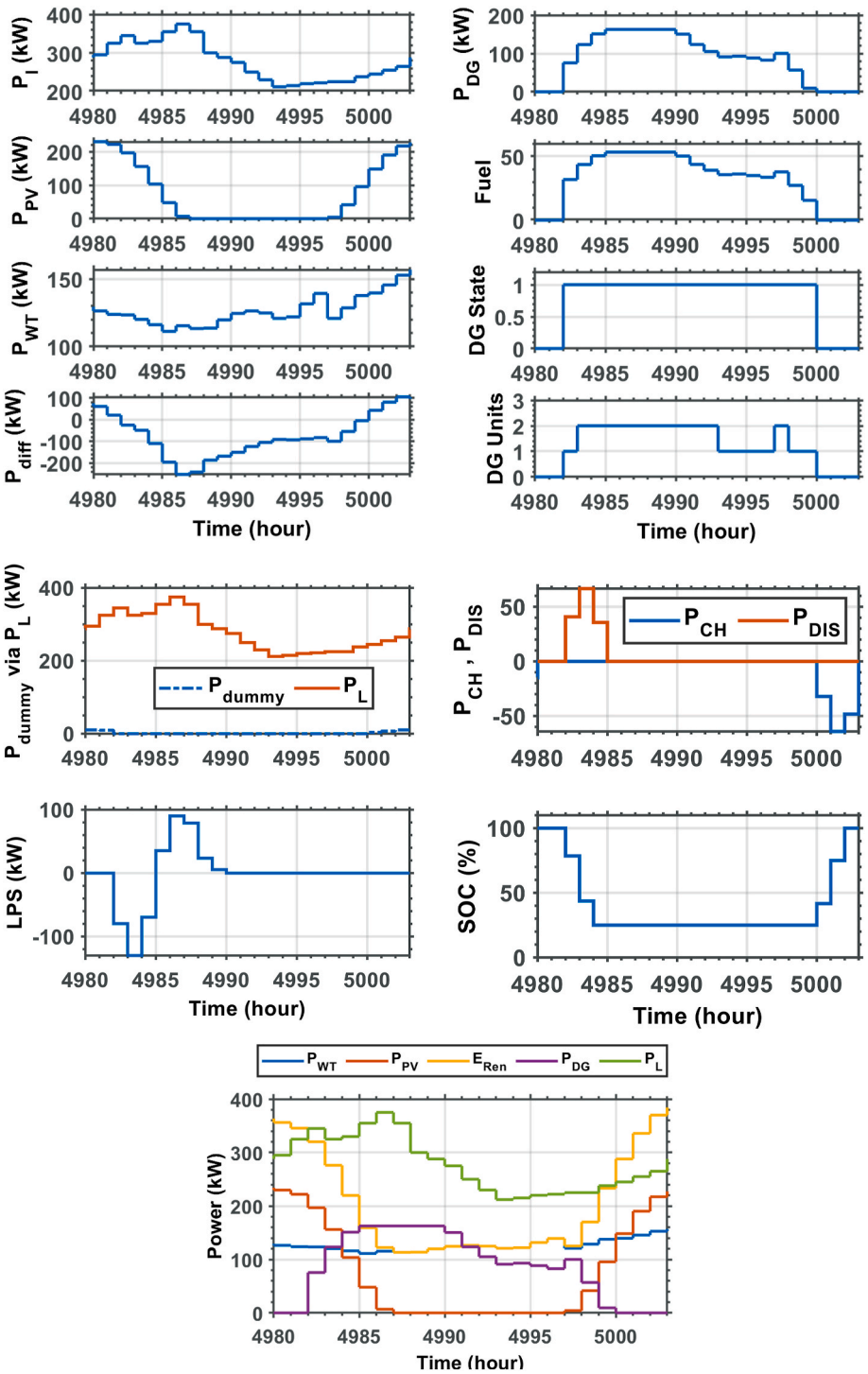

Fig. 16. Results of one day of simulation in August via the DMOA.

- The PV/BESS microgrid configuration results in the smallest value of the LCOE of 0.038, whereas the LPSP has the largest value of 0.679. On the other hand, the PV/WT/BESS/DG microgrid configuration results in an LPSP value of 1.9×10^{-8}%, with an LCOE value of 0.199 USD/kWh. The recommended configuration from a practical point of view is the PV/WT/BESS/DG, which ensures that the load demand is met.
- The results show that the configuration-based SSA gives the minimum LCOE, but the values of the LPSP and dummy load are larger than those of DOMA. Moreover, the two values of the LPSP with the SSA and DOMA are within the predefined limits.
- The performance of the optimization algorithms serves as a critical criterion for identifying the best algorithm, with a particular focus on convergence speed and reliability. This is assessed through multiple individual runs of the optimization problem. Our findings indicate that the differential optimization multiagent (DOMA) algorithm has the best convergence characteristics. Furthermore, the reliability and statistical results consistently demonstrate its superiority. Therefore, we strongly recommend the DOMA algorithm for this application.

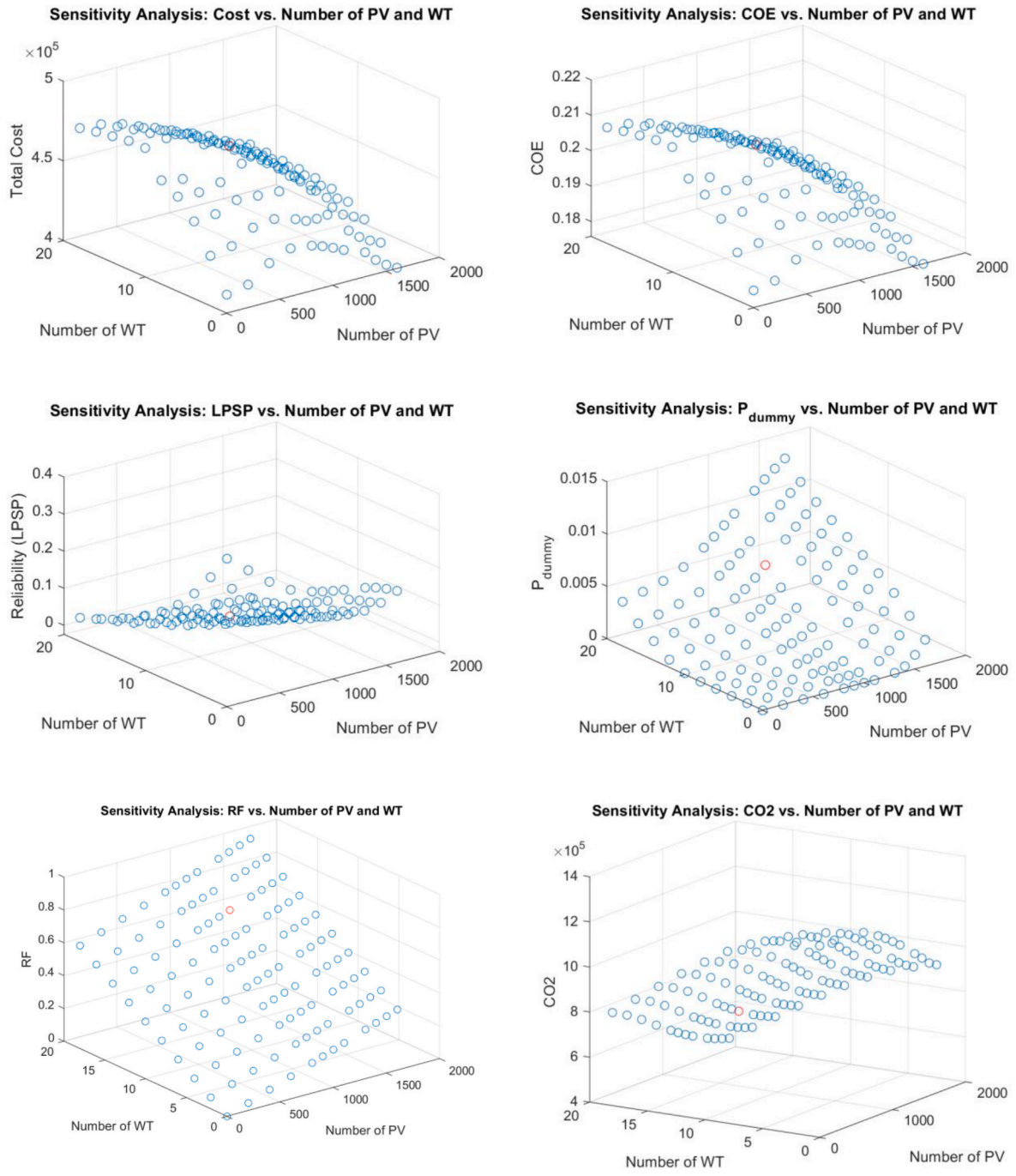

Fig. 17. Sensitivity analysis considering the variation in the PV and WT at fixed values of the DG and battery.

4.10. Limitations

This study focuses primarily on microgrid optimization using real data, rather than incorporating forecasting techniques, which introduces limitations in accurately predicting renewable energy generation and demand. Although the integration of renewable energy sources and energy storage systems is considered, the model does not fully address the uncertainties and fluctuations inherent in renewable energy production. Additionally, the research does not provide an in-depth analysis of the dynamic interaction between microgrids and larger utility grids, which could impact the scalability and interoperability of the proposed solutions. Furthermore, the study lacks a thorough examination of the integration of fast charging and hydrogen refuelling stations, which is vital for improving energy mobility options in rural areas. Another limitation of the paper is the focus on BESSs without considering alternative storage technologies such as hydro pumped storage, fuel cells, flywheels, supercapacitors, and thermal storage, which may offer more environmentally sustainable options in certain contexts.

5. Conclusions

In this work, various microgrid configurations featuring photovoltaic and wind power plants and BESS systems, both with and without backup diesel generators, have been optimally designed and compared to optimize renewable energy systems in Najran city/Saudi Arabia. In addition, this paper represents the first application of DMOA in optimizing the design of renewable energy sources (RESs), encompassing WT/PV/DG

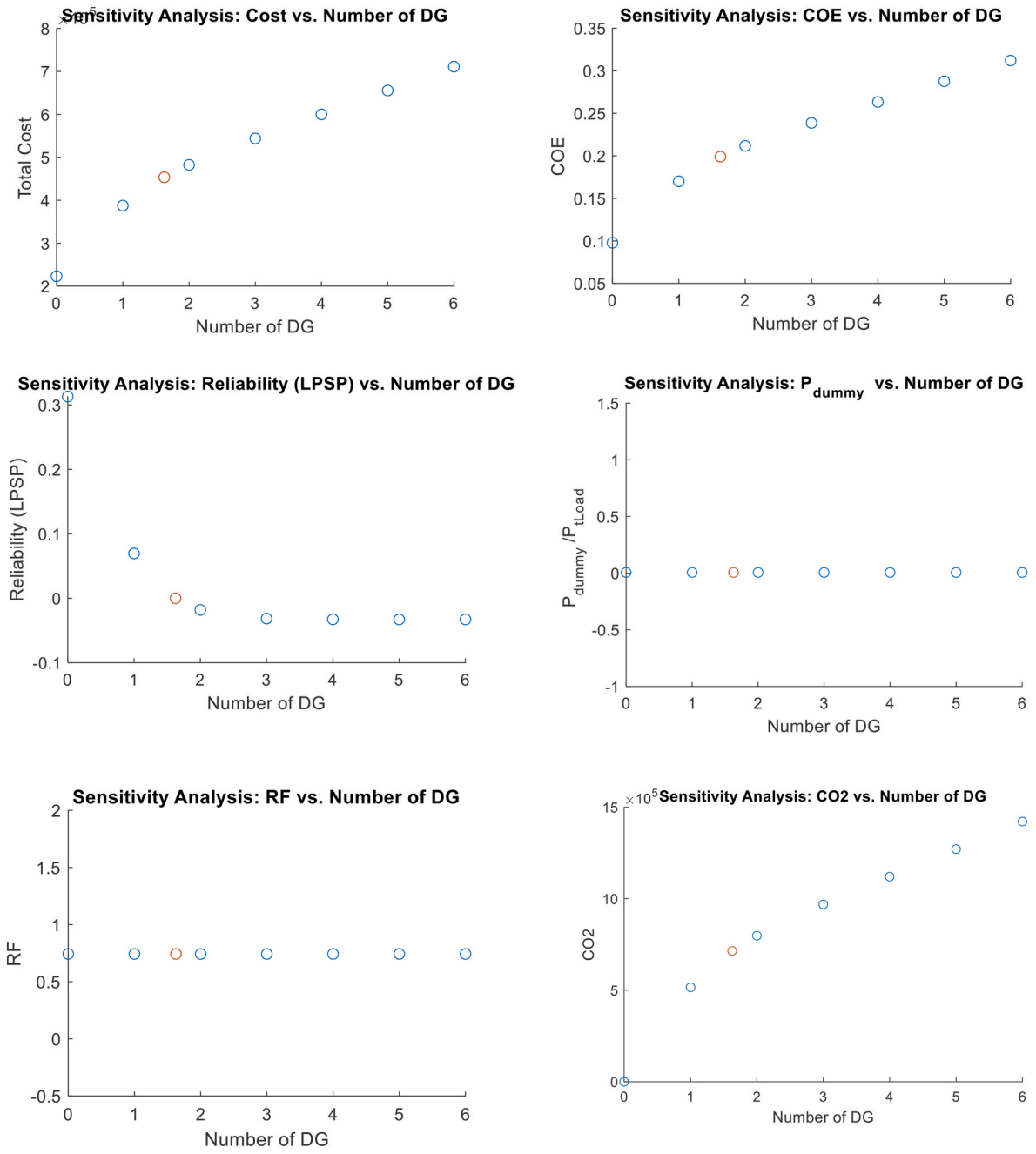

Fig. 18. Sensitivity analysis considering the variation in the number of DGs at fixed values of the PV, WT and battery.

RESs, as well as a BESS. Furthermore, the effectiveness of a hybrid energy system's optimal configuration has been confirmed through the implementation of two optimization algorithms, the WOA and SSA. The process occurred in various phases. Initially, a comprehensive model for the energy management system was formulated. Three different WOA, SSA, and DMOA algorithms are subsequently utilized to minimize the LPSP and LCOE, with the aim of determining the optimal energy system configuration. To assess the feasibility of this approach, a case study is conducted to evaluate the optimal design of the energy system by applying these optimization techniques. The optimization problem was addressed via MATLAB software. The results of these studies revealed that the DMOA outperformed the other algorithms, indicating significant progress in the field. Attaining the optimal value of the objective function 0.2 results in the lowest COE of 0.19 USD/kWh. The SSA and WOA yielded LCOE values of 0.19 USD/kWh. Furthermore, the fuel costs associated with the proposed hybrid system are lower than those associated with alternative methods, as evidenced by the energy cost derived from the DMOA method. The simulation results demonstrate that the DMOA exhibits superior accuracy and promising performance compared with the WOA and SSA. In addition, the statistical analysis confirmed that the applied optimization techniques exhibit adequate performance stability, with the DMOA considered the superior algorithm. In future work, the studied problem can be formulated as a multiobjective optimization problem with enhanced performance by using a hybrid optimization algorithm considering the uncertainty of RE availability. Moreover, future research in the field of microgrids should prioritize the development of advanced forecasting techniques to improve the accuracy of renewable energy generation predictions. Furthermore, advanced methods for optimizing load prioritization, such as real-time algorithms, can be explored to expand decision-making during power

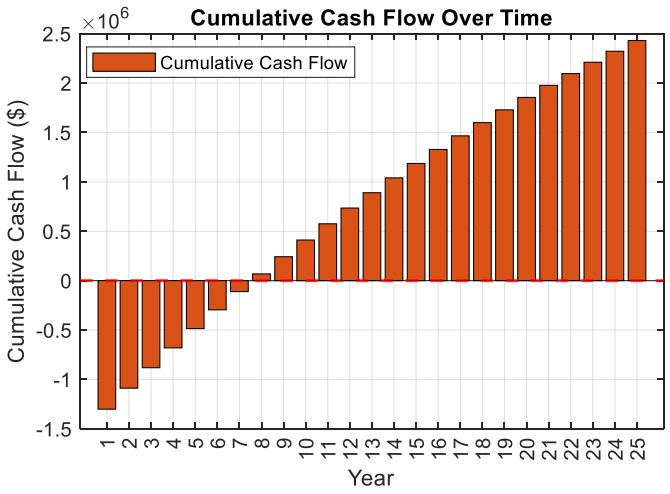

Fig. 19. payback periods of the optimal configured RES.

Table 8
Comparison of the findings of the current study with those of previous studies.

Ref	Configurations	Optimization Method	Site	LCOE (US $/kWh)
[47]	PV/Wind/BESS	HOMER	Abha, Saudi Arabia	0.614
[48]	PV/WT/DG/BESS	IGWO	El-Baharyia oasis, Egypt	0.2158
[33]	PV/Wind/DG/BESS	IAOA	El Kjharga oasis, Egypt	0.2606
[49]	PV/WT/FC	ISCA	Gonbad, Iran	0.87
[50]	PV/WT/FC	FPA	Ardabil, Iran	0.52
[34]	PV/WT/Tid/BESS	CSA	Fuxin, Northeast China	0.2045
[51]	PV/wind/DG/BESS	HOMER	Kudu village, Nigeria	0.259
[52]	PV/WT/DG/BESS	GOA	Yobe, Nigeria	0.3656
[53]	WT/DG/BESS	HPSODE-FAM	Chinese island, Jiuduansha	0.056
Outlined	PV/WT/BESS/DG	DMOA	Najran, KSA	0.199
Outlined	PV/WT/BESS	DMOA	Najran, KSA	0.098
Outlined	PV/BESS	DMOA	Najran, KSA	0.038

shortfalls.

CRediT authorship contribution statement

Saleh Al Dawsari: Writing – original draft, Validation, Software, Methodology, Data curation. **Fatih Anayi:** Supervision, Methodology, Investigation, Formal analysis. **Michael Packianather:** Supervision, Software.

Declaration of Competing interest

None of the authors have a conflict of interest to disclose.

Data availability

The data that has been used is confidential.

References

[1] Ahmad M, Khan I, Shahzad Khan MQ, Jabeen G, Jabeen HS, Işık C. Households' perception-based factors influencing biogas adoption: innovation diffusion framework. Energy Jan. 2023;263. https://doi.org/10.1016/j.energy.2022.126155.
[2] I. - International Energy Agency. Renewables 2022. www.iea.org. [Accessed 4 October 2024].
[3] Jabeen G, Ahmad M, Zhang Q. Towards sustainable environment: why green energy technology diffusion is sluggish in South Africa? Environ Sci Pollut Control Ser Feb. 2023;30(9):22653–67. https://doi.org/10.1007/s11356-022-23642-0.
[4] International Renewable Energy Agency. "Renewable capacity highlights," irena. 2021. April, p. 11 April.
[5] International Renewable Energy Agency. RENEWABLE ENERGY STATISTICS 2022 STATISTIQUES D'ÉNERGIE RENOUVELABLE 2022 ESTADÍSTICAS DE ENERGÍA RENOVABLE 2022 about IRENA [Online]. Available: www.irena.org; 2022.
[6] Jabeen G, Ahmad M, Zhang Q. Perceived critical factors affecting consumers' intention to purchase renewable generation technologies: rural-urban heterogeneity. Energy 2021;218(Mar). https://doi.org/10.1016/j.energy.2020.119494.
[7] International Trade Administration. "Saudi Arabia Renewable Energy,". 2021. p. 58 [Online]. Available: https://www.trade.gov/market-intelligence/saudi-arabia-renewable-energy. [Accessed 13 October 2024].
[8] Climate and energy benchmark - electric utilities [Online]. Available, https://www.worldbenchmarkingalliance.org/publication/electric-utilities/companies/saudi-electricity-company-sec-2/. [Accessed 25 June 2024].
[9] Dykes K, et al. Opportunities for research and development of hybrid power plants. May; 2020 [Online]. Available: https://www.osti.gov/servlets/purl/1659803/.
[10] Yu A, Li Z, Liu P. Rural integrated energy system based on bibliometric analysis: a review of recent progress. Processes 2024;12(1):176. https://doi.org/10.3390/pr12010176.
[11] Thirumalai SK, Karthick A, Dhal PK, Pundir S. Photovoltaic-wind-battery and diesel generator-based hybrid energy system for residential buildings in smart city Coimbatore. Environ Sci Pollut Control Ser 2024;31(9):14229–38. https://doi.org/10.1007/s11356-024-32071-0.
[12] Aziz AS, Tajuddin MFN, Adzman MR, Azmi A, Ramli MAM. Optimization and sensitivity analysis of standalone hybrid energy systems for rural electrification: a case study of Iraq. Renew Energy Aug. 2019;138:775–92. https://doi.org/10.1016/j.renene.2019.02.004.
[13] Shezan SA, Hasan KN, Rahman A, Datta M, Datta U. Selection of appropriate dispatch strategies for effective planning and operation of a microgrid. Energies Nov. 2021;14(21). https://doi.org/10.3390/en14217217.
[14] Elkadeem MR, Kotb KM, Ullah Z, Atiya EG, Dán A, Wang S. A two-stage multi-attribute analysis method for city-integrated hybrid mini-grid design. Sustain Cities Soc 2021;65(Feb). https://doi.org/10.1016/j.scs.2020.102603.
[15] Shezan SA. Feasibility analysis of an islanded hybrid wind-diesel-battery microgrid with voltage and power response for offshore Islands. J Clean Prod 2021;288(Mar). https://doi.org/10.1016/j.jclepro.2020.125568.
[16] Toopshekan A, Ahmadi E, Abedian A, Vaziri Rad MA. Techno-economic analysis, optimization, and dispatch strategy development for renewable energy systems equipped with Internet of Things technology. Energy 2024;296:131176. https://doi.org/10.1016/j.energy.2024.131176.
[17] Hasan S, Islam Meem A, Saiful Islam M, Sabrina Proma S, Kumar Mitra S. Comparative techno-economic analyses and optimization of standalone and grid-tied renewable energy systems for South Asia and Sub-Saharan Africa. Results in Engineering 2024;21:101964. https://doi.org/10.1016/j.rineng.2024.101964.
[18] Kumar PH, Gopi RR, Rajarajan R, Vaishali NB, Vasavi K, Kumar P S. Prefeasibility techno-economic analysis of hybrid renewable energy system. e-Prime - Advances in Electrical Engineering, Electronics and Energy 2024;7:100443. https://doi.org/10.1016/j.prime.2024.100443.
[19] Ming M, Wang R, Zha Y, Zhang T. Multi-objective optimization of hybrid renewable energy system using an enhanced multi-objective evolutionary algorithm. Energies 2017;10(5). https://doi.org/10.3390/en10050674.
[20] Wang R, Xiong J, fan He M, Gao L, Wang L. Multi-objective optimal design of hybrid renewable energy system under multiple scenarios. Renew Energy May 2020;151:226–37. https://doi.org/10.1016/j.renene.2019.11.015.
[21] Zaki Diab AA, Sultan HM, Mohamed IS, Kuznetsov Oleg N, Do TD. Application of different optimization algorithms for optimal sizing of pv/wind/diesel/battery storage stand-alone hybrid microgrid. IEEE Access 2019;7:119223–45. https://doi.org/10.1109/ACCESS.2019.2936656.
[22] al Busaidi AS, Kazem HA, Al-Badi AH, Farooq Khan M. A review of optimum sizing of hybrid PV-Wind renewable energy systems in Oman. Renew Sustain Energy Rev 2016;53:185–93. https://doi.org/10.1016/j.rser.2015.08.039.
[23] Kaur R, Krishnasamy V, Kandasamy NK. Optimal sizing of wind–PV-based DC microgrid for telecom power supply in remote areas. IET Renew Power Gener May 2018;12(7):859–66. https://doi.org/10.1049/iet-rpg.2017.0480.
[24] Nemouchi W, Amrane Y, Nemouchi H. Optimal sizing design of stand- alone hybrid system using a fuzzy PSO. In: Lecture Notes in networks and systems. Springer Science and Business Media Deutschland GmbH; 2022. p. 100–10. https://doi.org/10.1007/978-3-030-92038-8_10.
[25] Yang D, Jiang C, Cai G, Huang N. Optimal sizing of a wind/solar/battery/diesel hybrid microgrid based on typical scenarios considering meteorological variability. IET Renew Power Gener Jul. 2019;13(9):1446–55. https://doi.org/10.1049/iet-rpg.2018.5944.
[26] Kaur R, Krishnasamy V, Kandasamy NK, Kumar S. Discrete multiobjective grey wolf algorithm based optimal sizing and sensitivity analysis of PV-Wind-Battery system for rural telecom towers. IEEE Syst J Mar. 2020;14(1):729–37. https://doi.org/10.1109/JSYST.2019.2912899.
[27] Lei G, Song H, Rodriguez D. Power generation cost minimization of the grid-connected hybrid renewable energy system through optimal sizing using the modified seagull optimization technique. Energy Rep Nov. 2020;6:3365–76. https://doi.org/10.1016/j.egyr.2020.11.249.

[28] El-Sattar HA, Kamel S, Sultan HM, Zawbaa HM, Jurado F. Optimal design of photovoltaic, biomass, fuel cell, hydrogen tank units and electrolyzer hybrid system for a remote area in Egypt. Energy Rep Nov. 2022;8:9506–27. https://doi.org/10.1016/j.egyr.2022.07.060.
[29] Khan A, Javaid N. Optimal sizing of a stand-alone photovoltaic, wind turbine and fuel cell systems. Comput Electr Eng Jul. 2020;85. https://doi.org/10.1016/j.compeleceng.2020.106682.
[30] Alturki FA, Awwad EM. Sizing and cost minimization of standalone hybrid wt/pv/biomass/pump-hydro storage-based energy systems. Energies Jan. 2021;14(2). https://doi.org/10.3390/en14020489.
[31] Güven AF, Yörükeren N, Samy MM. Design optimization of a stand-alone green energy system of university campus based on Jaya-Harmony Search and Ant Colony Optimization algorithms approaches. Energy 2022;253(Aug). https://doi.org/10.1016/j.energy.2022.124089.
[32] Ashraf MA, Liu Z, Alizadeh A, Nojavan S, Jermsittiparsert K, Zhang D. Designing an optimized configuration for a hybrid PV/Diesel/Battery Energy System based on metaheuristics: a case study on Gobi Desert. J Clean Prod Oct. 2020;270. https://doi.org/10.1016/j.jclepro.2020.122467.
[33] Kharrich M, Abualigah L, Kamel S, AbdEl-Sattar H, Tostado-Véliz M. An improved arithmetic optimization algorithm for design of a microgrid with energy storage system: case study of El kharga oasis, Egypt. J Energy Storage 2022;51(Jul). https://doi.org/10.1016/j.est.2022.104343.
[34] Zhou J, Xu Z. Optimal sizing design and integrated cost-benefit assessment of stand-alone microgrid system with different energy storage employing chameleon swarm algorithm: a rural case in Northeast China. Renew Energy Jan. 2023;202:1110–37. https://doi.org/10.1016/j.renene.2022.12.005.
[35] Mohammadi M, Hosseinian SH, Gharehpetian GB. Optimization of hybrid solar energy sources/wind turbine systems integrated to utility grids as microgrid (MG) under pool/bilateral/hybrid electricity market using PSO. Sol Energy Jan. 2012;86(1):112–25. https://doi.org/10.1016/j.solener.2011.09.011.
[36] Rezk H, et al. Multicriteria decision-making to determine the optimal energy management strategy of hybrid PV–diesel battery-based desalination system. Sustainability Apr. 2021;13(8). https://doi.org/10.3390/su13084202.
[37] Zhang W, Maleki A, Rosen MA. A heuristic-based approach for optimizing a small independent solar and wind hybrid power scheme incorporating load forecasting. J Clean Prod Dec. 2019;241. https://doi.org/10.1016/j.jclepro.2019.117920.
[38] Abdelkader A, Rabeh A, Mohamed Ali D, Mohamed J. Multi-objective genetic algorithm based sizing optimization of a stand-alone wind/PV power supply system with enhanced battery/supercapacitor hybrid energy storage. Energy Nov. 2018;163:351–63. https://doi.org/10.1016/j.energy.2018.08.135.
[39] Caballero F, Sauma E, Yanine F. Business optimal design of a grid-connected hybrid PV (photovoltaic)-wind energy system without energy storage for an Easter Island's block. Energy Nov. 2013;61:248–61. https://doi.org/10.1016/j.energy.2013.08.030.
[40] Agushaka JO, Ezugwu AE, Abualigah L. Dwarf mongoose optimization algorithm. Comput Methods Appl Mech Eng 2022;391(Mar). https://doi.org/10.1016/j.cma.2022.114570.
[41] Kottek M, Grieser J, Beck C, Rudolf B, Rubel F. World map of the Köppen-Geiger climate classification updated. Meteorol Z Jun. 2006;15(3):259–63. https://doi.org/10.1127/0941-2948/2006/0130.
[42] Future Saudi cities programme city profiles series: najran [Online]. Available: www.momra.gov.sa; 2019.
[43] Albraheem L, AlAwlaqi L. Geospatial analysis of wind energy plant in Saudi Arabia using a GIS-AHP technique. Energy Rep Dec. 2023;9:5878–98. https://doi.org/10.1016/j.egyr.2023.05.032.
[44] Global solar atlas [Online]. Available, https://globalsolaratlas.info/pages/contact. [Accessed 15 November 2023].
[45] Mirjalili S, Lewis A. The whale optimization algorithm. Adv Eng Software May 2016;95:51–67. https://doi.org/10.1016/j.advengsoft.2016.01.008.
[46] Mirjalili S, Gandomi AH, Mirjalili SZ, Saremi S, Faris H, Mirjalili SM. Salp Swarm Algorithm: a bio-inspired optimizer for engineering design problems. Adv Eng Software Dec. 2017;114:163–91. https://doi.org/10.1016/j.advengsoft.2017.07.002.
[47] Al-Sharafi A, Sahin AZ, Ayar T, Yilbas BS. Techno-economic analysis and optimization of solar and wind energy systems for power generation and hydrogen production in Saudi Arabia. Elsevier Ltd.; Mar. 01, 2017. https://doi.org/10.1016/j.rser.2016.11.157.
[48] Mahmoud FS, et al. Optimal sizing of smart hybrid renewable energy system using different optimization algorithms. Energy Rep Nov. 2022;8:4935–56. https://doi.org/10.1016/j.egyr.2022.03.197.
[49] Jahannoush M, Arabi Nowdeh S. Optimal designing and management of a stand-alone hybrid energy system using meta-heuristic improved sine–cosine algorithm for Recreational Center, case study for Iran country. Applied Soft Computing Journal 2020;96(Nov). https://doi.org/10.1016/j.asoc.2020.106611.
[50] Hadidian Moghaddam MJ, Kalam A, Nowdeh SA, Ahmadi A, Babanezhad M, Saha S. Optimal sizing and energy management of stand-alone hybrid photovoltaic/wind system based on hydrogen storage considering LOEE and LOLE reliability indices using flower pollination algorithm. Renew Energy May 2019;135:1412–34. https://doi.org/10.1016/j.renene.2018.09.078.
[51] Oladigbolu JO, Al-Turki YA, Olatomiwa L. Comparative study and sensitivity analysis of a standalone hybrid energy system for electrification of rural healthcare facility in Nigeria. Alex Eng J Dec. 2021;60(6):5547–65. https://doi.org/10.1016/j.aej.2021.04.042.
[52] Bukar AL, Tan CW, Lau KY. Optimal sizing of an autonomous photovoltaic/wind/battery/diesel generator microgrid using grasshopper optimization algorithm. Sol Energy Aug. 2019;188:685–96. https://doi.org/10.1016/j.solener.2019.06.050.
[53] Singh P, Pandit M, Srivastava L. Multi-objective optimal sizing of hybrid micro-grid system using an integrated intelligent technique. Energy 2023;269(Apr). https://doi.org/10.1016/j.energy.2023.126756.